Computational Studies of [NiFe] and [FeFe] Hydrogenases

Per E. M. Siegbahn*

Department of Biophysics, Arrhenius Laboratory, Stockholm University, SE-106 91, Stockholm, Sweden

Jesse W. Tye and Michael B. Hall*

Department of Chemistry, Texas A&M University, College Station, Texas 77843-3255

Received January 4, 2007

Contents

1. Introduction

Dihydrogen has the potential to act as a "clean'' alternative to fossil fuels.[1] The oxidation of dihydrogen, either electrochemically or via combustion, leads only to the production of water. Unfortunately, the best synthetic catalysts for H_2 production and consumption utilize the expensive and relatively scarce noble metal platinum. The hydrogenase enzymes hold out the hope of using the base metals iron and nickel for these processes.

This review will focus on computational studies of H−H bond cleavage and formation by the hydrogenase enzymes. In all cases so far, density functional theory (DFT) has been used in these studies. Various aspects of the hydrogenase enzymes have been the subject of a number of recent reviews.[2−22] The activation of dihydrogen by discrete, synthetic transition-metal complexes has also been the subject of a number of excellent reviews.[23−40]

* To whom correspondence should be addressed. Per E. M. Siegbahn. E-mail: ps@physto.se; telephone: +46-8-16 12 63; fax: +46-8-55 37 86 01. Michael B. Hall. Email: mbhall@tamu.edu; fax: (+1) 979-845-4719.

Table 1. Bond Dissociation Energies for H−X Bonds

bond type	average BDE[a]
H−F	135(1)[b]
H−O	109.60(4)
H−H	103.25(1)
H−Cl	102.3(1)
H−C	98.3(8)
H−N	92(2)

[a] Data from ref 41 in kcal/mol. [b] Error in last digit is given parenthetically.

Table 2. Proton Dissociation Constants for Several Compounds in Organic Solvents

acid	pK_a	solvent	ref
H**H**	49	THF	43
Ph_3C**H**	44	THF	43
Cyclohexane-O**H**	38	THF	43
Ph_2P**H**	35	THF	43
CH_3COO**H**	22.3	CH_3CN	44
$CH_3(C_6H_4)SO_3$**H**	8.0	CH_3CN	45
CF_3SO_3**H**	2.60	CH_3CN	45

The activation of dihydrogen is generally a difficult process. The H_2 molecule is, in fact, so stable that it was used as an "inert'' gas in early air-free chemistry. The following physical properties of H_2 combine to make it a very unreactive molecule: (1) The H−H bond is remarkably strong. (2) The H_2 molecule is completely nonpolar. (3) The H_2 molecule is a very poor acid.

The amount of energy required for homolytic cleavage of the H−H bond into two hydrogen atoms is +103.25(1) kcal/mol.[41] As shown in Table 1, this value places the H−H bond among the strongest single bonds.[42] Because most new H−X bonds will generally be weaker than the H−H bond, there is often little or no thermodynamic driving force for the cleavage of the H−H bond.

The uncatalyzed heterolytic cleavage of the H−H bond is also difficult. The strength of the H−H bond and its lack of polarity contribute to the poor kinetic and thermodynamic acidity of H_2. The pK_a values for a series of monoprotic "acids'', dissolved in either tetrahydrofuran or acetonitrile solvent, are given in Table 2. Dihydrogen with an estimated pK_a of 49 in tetrahydrofuran solvent is among the weakest acids.

The H_2 ase enzymes may be broadly classified by specifying the transition-metal content of their active sites. The three main classes of hydrogenase enzymes are the nickel−iron ([NiFe]),[46−48] iron−iron ([FeFe]),[49,50] and the

10.1021/cr050185y CCC: $65.00
Published on Web 10/10/2007

Per E. M. Siegbahn was born in Stockholm, Sweden. He did his undergraduate studies at Uppsala University and received his Ph.D. degree at Stockholm University, in 1973 (with Björn Roos). He was a postdoctoral fellow at the University of California, Berkeley (with Henry F. Schaefer III), and at IBM, San Jose (with Bowen Liu). He returned to Stockholm and has remained ever since. His interests have varied over the years from the development of ab initio quantum chemical methods, to the applications on gas-phase reactions of small molecules, to models of heterogeneous catalysts, to the present interest in mechanisms for redox-active enzymes.

Jesse W. Tye was born in Kentucky and graduated from the University of Kentucky with a B.S. degree in Chemistry in 2001. He graduated with a Ph.D. degree in Chemistry from Texas A&M University in 2006. His Ph.D. research was conducted under the joint direction of Profs. Marcetta Y. Darensbourg and Michael B. Hall and involved experimental and computational studies of di-iron complexes related to the active site of the iron–iron hydrogenase enzyme. He is currently a postdoctoral research associate in Prof. John F. Hartwig's laboratory of Illinois Urbana—Champaign. His postdoctoral research focuses on experimental and computational studies of copper-catalyzed C–N bond-forming reactions.

so-called iron−sulfur cluster-free hydrogenases, which until recently were thought to be "metal-free''.[51−54] The [NiFe] enzymes are primarily utilized for hydrogen oxidation, whereas the [FeFe] enzymes are primarily utilized for proton reduction. The iron−sulfur cluster-free hydrogenases are H_2-utilizing enzymes, which activate dihydrogen for use in catabolic processes within the cell but do not catalyze H^+ reduction or H_2 oxidation. Certain organisms also contain H_2-sensing hydrogenases, which regulate H_2 oxidation and/or H^+ reduction in these organisms.[55,56]

2. [NiFe] Hydrogenases

2.1. Structure and Active Site Models

The first crystal structure of a Ni−Fe hydrogenase was obtained for the oxidized form of *Desulfovibrio gigas* at a

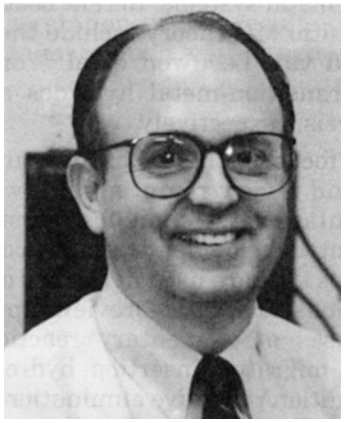

Professor Hall was born in Pennsylvania and graduated from Juniata College with a B.S. degree in Chemistry in 1966. After completing his Ph.D. degree with Richard Fenske at the University of Wisconsin in 1971, he accepted an AEI fellowship to study ab initio quantum chemistry with Ian Hillier at the University of Manchester, England. He accepted an appointment as Assistant Professor of Chemistry at Texas A&M University in 1975, rose through the ranks, and served as Head of the Department from 1986 to 1994. He currently directs the Laboratory for Molecular Simulation and serves as Associate Dean for Research and Information Technology in the College of Science. His research interests are primarily directed toward understanding chemical structures and reactions through the application of state-of-the-art quantum calculations. He serves on the Editorial Advisory Board of *Theoretical Chemistry Accounts*.

resolution of 2.85 Å.[57,58] In the following years, X-ray structures from other organisms were also obtained, for the oxidized form of *Desulfovibrio fructosovorans*,[59] for the oxidized and reduced forms of *Desulfovibrio vulgaris* (Miyazaki F),[60−62] and for the reduced form of *Desulfovibrio baculatus*,[47] where the last one is the first Ni−Fe−Se hydrogenase structure (see Figure 1). Quite recently, two different studies have obtained additional information on the oxidized forms of the [NiFe] hydrogenases.[63,64]

The most surprising feature of the Ni−Fe active site in all these hydrogenases is the ligand structure around iron with three diatomic ligands. The identity of these ligands as two CN and one CO ligand, which is unique for a biochemical system, was demonstrated by infrared spectroscopy for *Allochromatium vinosum*.[65] There are also four cysteine ligands, where two are bridging between the metals and two are terminal nickel ligands. In the Ni−Fe−Se enzyme, selenium is substituted for sulfur in one of these terminal ligands, Cys492, indicating a special role in the mechanism for this cysteine.

Because hydrogenases are enzymes where the purpose is to make a charge separation (or the reverse), there have to be pathways leading in different directions for the electrons and the protons produced. The electron-transfer pathway is easy to identify going over one or more Fe−S clusters. The most nearby Fe−S cluster is shown in Figure 1. At least two possible proton-transfer pathways have been identified. One of these pathways starts at CysSe492 and goes over Glu23 and several conserved water molecules, of which two are shown in the figure, and leads to a Mg complex (not shown) near the surface.[19] Another pathway starts at the bridging Cys495 ligand and goes straight out to the surface via hydrogen bonds over His77, His430, and Tyr442. This pathway is similar to the one suggested for Ni−CO dehydrogenase.[66,67] Other proton-transfer pathways are also possible.

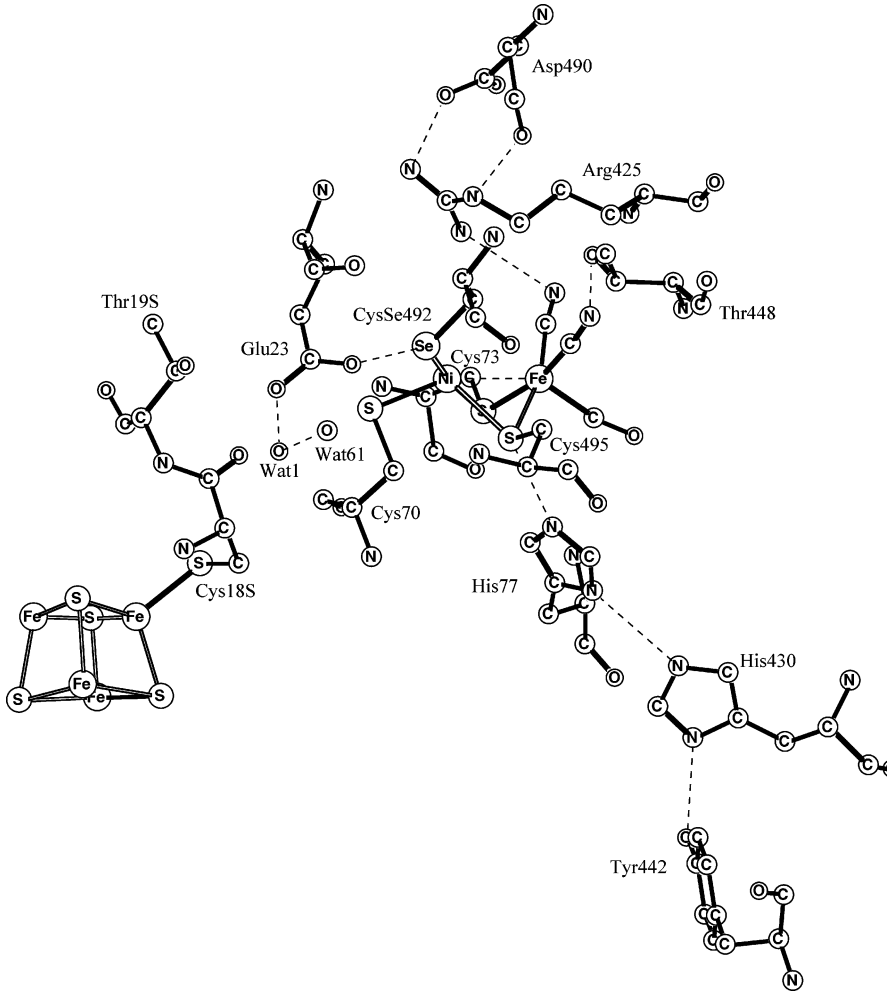

Figure 1. X-ray structure for the reduced form of the [NiFe] hydrogenase from *Desulfovibrio baculatus*.

2.1.1. Observed States

Extensive EPR spectroscopic studies indicate the accessibility of several different enzyme states. These states can be divided into two classes. Those which are observed in connection with the enzyme in its active form in the presence of dihydrogen belongs to the first class. These states are all termed reduced, independently of the oxidation states observed. The resting state in the active catalytic cycle is termed Ni_a-C* and shows an EPR signal. Reduction of Ni_a-C* yields Ni_a-SR, and oxidation yields Ni_a-S, both EPR-silent forms. The X-ray structure in Figure 1 has been identified as a mixture of the Ni_a-C*, Ni_a-S, and Ni_a-SR states. The second class of states is observed after exposure to air and are termed oxidized states. X-ray structures have been obtained for two of these states, as described above. One of them is Ni-A, termed the inactive, unready form because the activation of this state may take hours. The recent X-ray analysis of Ni-A suggests the presence of a bridging, protonated peroxide, bidentately bound to nickel. The other form is Ni-B, termed the inactive, ready enzyme because it can be activated in seconds by H_2 or by adding electrons and protons. Ni-B is suggested to have a bridging hydroxide. Ni-A and Ni-B are both EPR-active doublet states. For both the reduced and the oxidized enzymes, several other states have been observed under varying conditions, but these will not be discussed in the present review.

2.1.2. Active Site Models

A variety of different models have been used in the different DFT studies of [NiFe] hydrogenases. All of these cannot be mentioned here, but three typical models of different size are shown in Figure 2. The numbering of the amino acids in these structures is that from *Desulfovibrio gigas*, which is different from the one in *Desulfovibrio baculatus* in Figure 1. In the minimal model A, only the directly liganding groups were included, apart from nickel, iron, and the substrate. This is the model by far most commonly used for DFT studies. In the medium size model B, also Glu25, His79, Arg476, and Asp541 are included. Glu25 is included because it is the first link to one of the suggested proton-transfer pathways. It also has a relatively strong hydrogen bond to Cys543, indicating that it is protonated. In the particular version of this model shown in the figure, the entire side chains of Glu25 and Cys543 were included in the model because these amino acids were considered likely to be directly involved in important proton transfers. For the other amino acids, only the functional groups were used in this particular model. The other amino acids included are His79 because it forms a hydrogen bond to one of the cysteines, Arg476 because it is charged and very close to the position of the substrate, and Asp541 to compensate for the charge of Arg476. Other amino acids that might have been considered for inclusion are those forming hydrogen bonds to the cyanides and also Asp114, which is present in the largest model C in the figure because

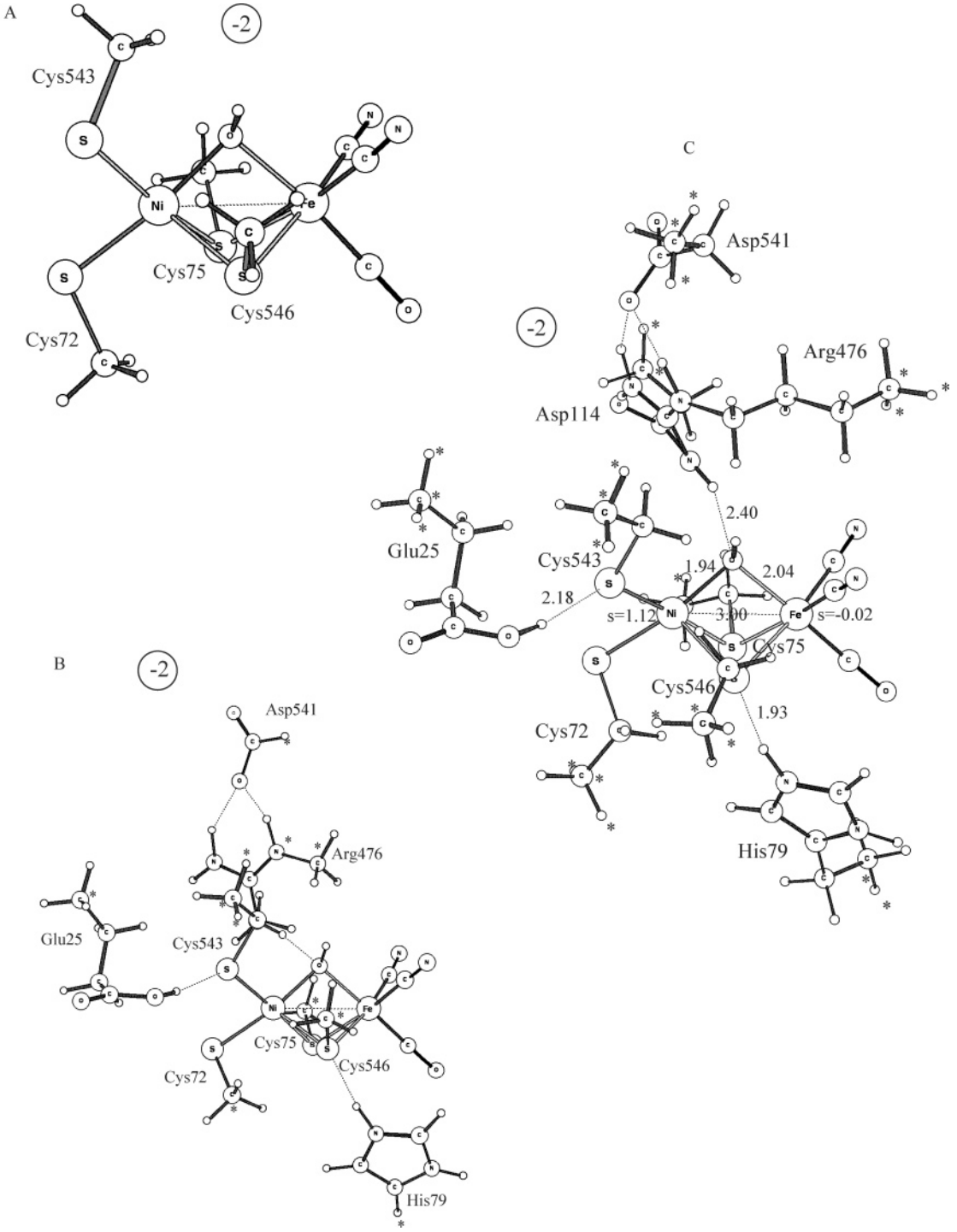

Figure 2. Three models used for the active site of [NiFe] hydrogenase. Positions frozen from the X-ray structure are marked with *. Note that the numbering of the amino acids is the one for *Desulfovibrio gigas* which is different from the one in Figure 1.

it forms a salt bridge to Arg476. A major principle difference between the minimal and medium size model in Figure 2 is that some of the amino acids are not directly bound to the metal in the larger model. To not allow an unreasonably large flexibility for these ligands, some point(s) of each of these amino acids must be kept frozen at the corresponding position of the X-ray structure, marked with a * in Figure 2. All other atoms in the models are fully optimized. This procedure is well tested for many enzyme active sites[68] but may turn out to have larger difficulties in this particular case, due to the unusually large number of charged amino acids. The charge states are normally chosen as those at pH = 7; i.e., carboxylates are usually negative, and arginine is positive. However, from a model study of the [NiFe] active site,[69] His79 and Glu25 were chosen to be protonated.

Calculations on [NiFe] hydrogenase have also been done using combined quantum mechanics, molecular mechanics (QM/MM) models, where the entire enzyme is included in the model. In these models, the QM part is approximately the size of the small model A in Figure 2. It should be emphasized that because compromises of this type have to be done the energetics using the QM/MM model is not necessarily more accurate than that obtained from a pure QM model like C in Figure 2, even though all atoms in the enzyme are included in the QM/MM model.[70] However, in the present case of [NiFe] hydrogenase, both QM/MM

studies performed have focused on structures, where QM/MM models should be superior even to large QM models. In one of these studies, the structures of the intermediates of the catalytic cycle were obtained and compared to experiments.[71] In the other one, a quantum refinement was made of the crystallographic data for the oxidized enzyme.[72]

2.1.3. Spin State of the Active Complex

The spin states of intermediates involved in an enzymatic mechanism are always an important issue. In the case of [NiFe] hydrogenases, there has been a considerable debate concerning the spin state of those intermediates in the dihydrogen activation cycle that have an even number of electrons, Ni_a-S and Ni_a-SR. The electronic ground state (singlet or triplet) of these Ni^{II} intermediates is still controversial. Parallel mode EPR,[73] saturation magnetization,[74] and UV−visible MCD studies[75] suggest singlet (diamagnetic) spin states, and recent L-edge X-ray adsorption spectroscopy[76] and DFT using the B3LYP functional[77] suggest that they could be triplet states. As discussed below, the structures of these intermediates are likely to have either a bridging hydride or no substrate at all.

The most careful theoretical analyses of the spin states of the Ni_a-S and Ni_a-SR have been performed by Bruschi et al.[78] They did DFT calculations using the nonhybrid (without exact exchange) BP86 functional and the hybrid (with exact exchange) B3LYP functional for models of these two states as well as for some nickel complexes where the spin states are known. It is well-known that B3LYP favors high-spin states in general, whereas nonhybrid methods favor low-spin states.[79] In fact, the singlet−triplet splitting generally depends linearly on the amount of exact exchange, and this is the case also for the Ni_a-S and Ni_a-SR states. From comparisons on a number of transition-metal complexes with different metals, it was found that an inclusion of 15% exchange is often optimal in this context.[79] This is closer to B3LYP which has 20% exact exchange than to BP86 which has no exact exchange. For Ni_a-S and Ni_a-SR, the sensitivity to the amount of exact exchange is unusually high, and B3LYP favors the triplet by about 5 kcal/mol while BP86 favors the singlet by 5−10 kcal/mol. Including 15% exact exchange leads to a splitting near zero, which should thus be the best, although rather uncertain, theoretical estimate at present. Remarkably, the computed singlet and triplet reaction energy profiles for [NiFe] hydrogenase are quite similar, so for a general energetic and structural discussion of the hydrogenase mechanism, the choice of spin state does not have a major impact. Most commonly, the singlet state has been chosen for the different DFT studies. The odd-electron systems are doublets.

The spin populations in the doublet and triplet states rarely show any spin on iron, indicating that iron nearly always stays Fe^{II} and has a low-spin coupling of its d-electrons. This is expected with the strong ligand field around iron mainly produced by the CN and CO ligands. It should be added that a low-spin coupling on iron is not common in biological systems and is mainly limited to heme systems. Nickel, on the other hand, takes on three different oxidation states in the processes discussed below. For the closed-shell singlet states, nickel is Ni^{II}. For the doublet states, nickel is mainly in the Ni^{III} state with a spin population close to one. However, in the catalytic cycle, nickel also takes on the oxidation state Ni^{I} with a spin population, 3d-population, and charge quite similar to the ones in Ni^{III}. The difference between Ni^{I} and Ni^{III} can therefore not be identified from its populations. Instead, the assignment of an oxidation state is based on normal counting conventions where cysteinates and CN ligands are given a charge of −1 and a hydride is also given a charge of −1. Given that iron is in the Fe^{II} state, the oxidation state of nickel is found by matching the total charge of the complex. The triplet state of nickel can appear under certain circumstances and has a spin population of about 1.5. In principle, Ni^{III} could also be in a quartet state with three spins. However, all attempts to converge a solution to Ni^{III}-Fe^{II} with three spins on nickel have so far failed and instead gave an additional spin on iron. The cysteinates also commonly carry some spin in the range 0.1−0.3 in both the triplet and the doublet states, but significantly higher spin populations indicating radical character may also occur under certain circumstances.

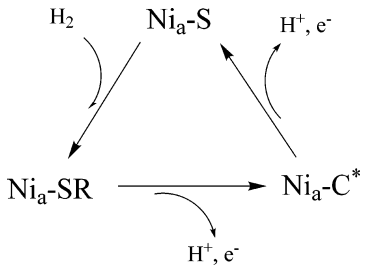

Figure 3. Active cycle of [NiFe] hydrogenases.

2.2. Reaction Mechanism of [NiFe] Hydrogenases

The active cycle of [NiFe] hydrogenases is usually illustrated by a scheme such as the one in Figure 3. It contains the three intermediate states observed experimentally, Ni_a-C*, Ni_a-S, and Ni_a-SR. Ni_a-C* is the resting state of the catalytic cycle, and it is EPR-active as illustrated by the * in its name. It is normally described as a $Ni^{III}Fe^{II}$ state. Ni_a-C* is connected to the other two states which are EPR-silent (as denoted with an S). These two states are usually described as $Ni^{II}Fe^{II}$. The Ni_a-SR is termed reduced because overall it has one more electron than Ni_a-C* and two more electrons than Ni_a-S. The $Ni^{III}Fe^{II}$, Ni_a-C*, state is reached upon oxidization of Ni_a-SR, which makes it clear that it is a reduced state. In contrast, Ni_a-S is obtained by oxidizing Ni_a-C*. Still its oxidation states are the same, $Ni^{II}Fe^{II}$, as the ones of Ni_a-SR. This may appear confusing, but there is in fact nothing strange in this because the $Ni^{III}Fe^{II}$ state of Ni_a-C* could be internally reduced to $Ni^{I}Fe^{II}$ by a hydride transfer before it is oxidized to Ni_a-S, as will be described below. To complete the cycle, Ni_a-SR can be reached by adding dihydrogen to Ni_a-S. This step is termed a reduction because electrons are added from dihydrogen, even though it does not change the oxidation states of the metals. As described above, the nomenclature with oxidized and reduced states used for hydrogenase is different from the one normally used in organometallic chemistry, where only the oxidation states count.

2.2.1. Mechanism for Dihydrogen Activation

Before the present understanding of the dihydrogen activation mechanism is summarized, a few words of caution are needed. In connection with the recent X-ray structures of the oxidized Ni-A state,[63,64] showing a bidentately bound peroxide species, it became evident that the modeling used in most studies of the mechanism of [NiFe] hydrogenase has not been satisfactory. All small model studies performed

suggested a quite different structure of Ni-A than the one eventually found experimentally. Furthermore, the energy difference between the preferred structure in the small models and the experimental one is quite substantial, on the order of 15 kcal/mol (see below). It is quite likely that the modeling problems for Ni-A are present also for the states involved in the mechanism of [NiFe] hydrogenase, and it would therefore not be surprising if an entirely different mechanism will eventually be found than any one of those described here.

The heterolytic cleavage of dihydrogen has been studied for [NiFe] hydrogenases by many groups using several different models. Due to the severe problems of using small models for the active site of [NiFe] hydrogenase mentioned above, the present review of the mechanism will start out from the results using the largest model so far.[69] It is important to clarify that this should not be interpreted as a suggestion that this study should give the right mechanism. On the contrary, much larger models than hitherto used are needed to convincingly model the mechanism, and significant modifications of the mechanism are likely to appear in such studies.

The first question investigated in the model studies was the oxidation state of the reactant for dihydrogen cleavage. Several different models were used, and the conclusion from the largest models is that it is most likely the $Ni^{II}Fe^{II}$ state that activates dihydrogen. This choice of oxidation states led to an energetically neutral potential surface, in contrast to choosing the $Ni^{III}Fe^{II}$ state, as will be described below. It should be added that the $Ni^{II}Fe^{II}$ state as the active state has been suggested experimentally[80] and was for that reason chosen in some theoretical studies of the hydrogenase mechanism.[71,81,82]

The choice of the $Ni^{II}Fe^{II}$ state is different from the conclusions drawn from some of the earlier studies using smaller models,[83−89] where the $Ni^{III}Fe^{II}$ state was suggested as the active state. This difference depends strongly on the model used. The main origin of the differences appears to be whether charged residues outside the first shell ligand sphere were included in the model or not. The choice of charge state of the [NiFe] core could be another reason for the differences. In the study described most in detail here, the charge of the core is −2 (see above), whereas in the early studies, it was neutral. These model differences have a surprisingly large effect on the potential curve for dihydrogen cleavage. With the smaller and neutral model, the H_2 cleavage is strongly endergonic for the $Ni^{II}Fe^{II}$ oxidation state but becomes exergonic for larger models with a charge of −2.

The next question investigated was where H_2 binds on the NiFe dimer. The largest model used to study the mechanism is shown in Figure 4. It should be noted that unusually large distortions of the geometry compared to the experimental structure were found during the reaction pathway, in spite of freezing some coordinates from experiments, which is why the results should be taken with some caution (see also the modeling problems of Ni-A). The result for the closed-shell singlet $Ni^{II}Fe^{II}$ state is that dihydrogen prefers to bind on iron, but this is only a local minimum. In fact, the binding was calculated to be endothermic by 6.2 kcal/mol with a surprising effect of +3.3 kcal/mol from zero-point vibrational effects (the energies discussed here have been recomputed using a large basis set, cc-pvtz(-f), combined with lacv3p** and differ therefore slightly from what was reported previously[69]). Entropy effects can be estimated to be nearly +10 kcal/mol but should to some extent be compensated by enzyme effects like van der Waals interactions,[90] here estimated to be −5 kcal/mol. For the construction of the energy diagram (see further below), an additional effect of +5.0 kcal/mol was therefore added, increasing the endergonicity of binding H_2 from +6.2 to +11.2 kcal/mol. A repulsive interaction between H_2 and the NiFe complex might at first sight appear as unreasonable for a system particularly designed to activate H_2, but the final energetics for the entire catalytic cycle of hydrogenase (see further below) does in fact make an endergonic binding of H_2 appear possible. On the other hand, it is still significant that there is a local minimum for binding H_2 on iron. This minimum implies a favorable electronic interaction between H_2 and the metals which will allow an effective cleavage of H_2 with a low barrier.

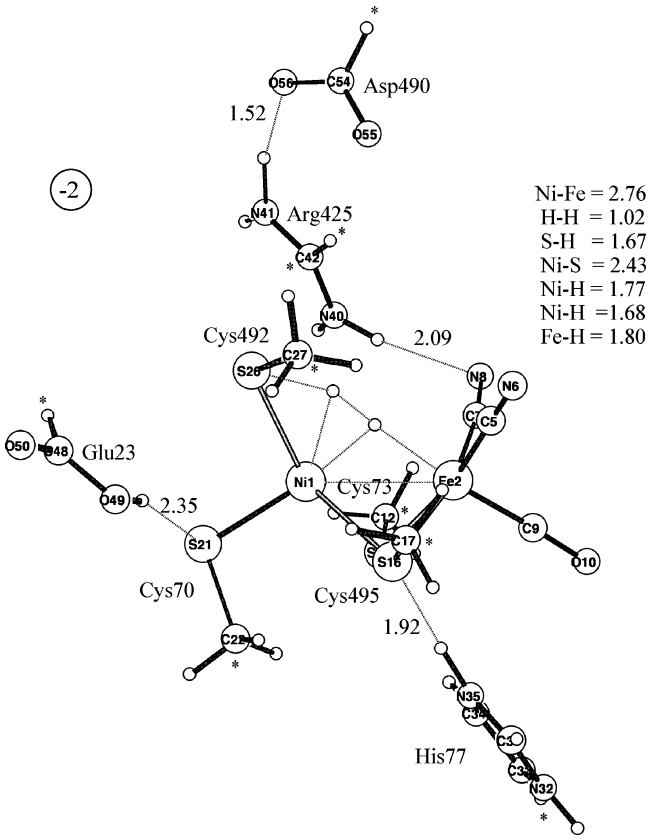

Figure 4. Optimized transition state for H−H bond cleavage in Ni−Fe hydrogenase. The oxidation states are Ni^{II} and Fe^{II}. Distances are given in Å. Atoms marked with * were kept frozen from the X-ray structure during the optimization. The numbering of the amino acids is from *Desulfovibrio baculatus* (see Figure 1).

The position of dihydrogen in the local minimum on iron is the same result as obtained in previous studies[83,86] but different from what has been suggested from experiments on the enzyme. Xenon binding experiments have located a likely path for dihydrogen transport to the active site which ends at nickel,[91,92] which was therefore suggested as the site for dihydrogen binding and activation. Also, X-ray crystal structures show that a CO-inhibitor binds at nickel, not at iron.[62] The nickel binding site was therefore carefully investigated for the singlet using the model in Figure 4, but no local minimum was found. From the experience of organometallic dihydrogen complexes, the iron site is, on the other hand, the expected site for dihydrogen binding.[24] This site for binding and activation would also give a natural

explanation for the unusual choice of iron ligands. These ligands force a low-spin coupling on iron which is ideal for activating dihydrogen.[93]

With dihydrogen bound on iron, there are essentially only two possible mechanisms for cleaving H_2 heterolytically. Both these mechanisms lead to a hydride bridging between iron and nickel. In the first mechanism, the proton goes to the terminal CysSe492, whereas in the other one, the proton goes to the bridging Cys495. In earlier studies, the bridging cleavage has been favored in actual transition-state optimizations,[83] but the terminal cleavage has also been suggested from structural considerations and optimizations.[86,88] For the model used for the calculations described here, the terminal mechanism was found to be favored by 3.5 kcal/mol due to the repulsion with the protonated His77 in the bridging pathway.[69] If His77 is unprotonated, the bridging pathway is instead preferred by 1.1 kcal/mol. The optimized transition-state (TS) structure for the terminal pathway is shown in Figure 4. The barrier counted from the dihydrogen minimum is only 1.4 kcal/mol, but with the large distortions found for the structure, this value could increase using a larger model. With the additional energy of 11.2 kcal/mol to reach the molecular minimum, the total barrier becomes 12.6 kcal/mol. Apart from the distortions, notable structural features are that the hydrogen bond from Glu23 shifts from Cys492 to Cys70 and that the hydrogens in this mechanism stay very close to nickel. The Ni−Fe distance shortens significantly by 0.3 Å from the molecular minimum to the TS. The reaction is exergonic by 2.6 kcal/mol, counted from a hydrogen molecule at a long distance from the NiFe complex. The reaction exergonicity compared to the local dihydrogen minimum is 13.8 kcal/mol.

The barrier for the alternative bridging pathway is higher than for the terminal pathway by 3.5 kcal/mol. In the process of cleaving H_2, the Ni−SCys495 distance increases significantly because the Ni−S bond is replaced by a Ni−H bond. The Ni−Fe bond distance remains essentially the same from the molecular minimum to the TS but then shortens due to the formation of the bridging hydride. The hydrogens remain close to both iron and nickel during the reaction. Again, substantial distortions of the structure were noted.

Because the barrier was found to be lower for the terminal pathway, it will be assumed that the reaction takes this route. The next step was then to remove one electron and one proton. The electron is likely to be removed first because the complex is negatively charged. To obtain an accurate value for the energy of removing a proton, or an electron, is a very difficult task because the effect of the surrounding enzyme is quite large and also depends on the charge distribution in detail. To obtain the energy required to remove a proton from the complex, an estimate of the binding energy of a proton to bulk water is also needed, which is even harder to obtain. For obtaining the energy required to remove an electron, the redox potentials of both the donor NiFe complex and the FeS acceptor complex are needed. To obtain calculated values for these energies, the most accurate procedure available is to use a QM/MM model. Even then, an accuracy better than 5 kcal/mol is difficult to achieve for a transition-metal containing enzyme like the present one. As will be discussed further below, the only attempt made to estimate these energies was by the use of a semiempirical procedure where the only requirement is to obtain the energy to remove a proton and electron simultaneously from the complex.[69] It should be noted that this does not imply that they should leave the complex in a concerted fashion. To obtain an accurate value to remove both an electron and a proton is much easier than removing them one at a time because the complex will not change its charge. The dielectric effects when the charge is not changed are typically 1−4 kcal/mol, and they can be as large as 25 kcal/mol when the charge is changed, illustrating the difference in the sensitivity to the surroundings. Furthermore, the redox potential of the FeS acceptor complex and the pK_a of bulk water are not needed in this procedure. From the bridging hydride product, the calculated cost to remove an electron (from nickel) and a proton from the terminal Cys492 is 59.3 kcal/mol. How this energy should be used to construct an energy diagram will be discussed below. As mentioned in a previous section, the electron-transfer pathway is easily identified from the X-ray structures, whereas for the proton transfers there are a few possibilities. For the terminal mechanism, the pathway suggested from the X-ray structure[19] is well suited because it is connected directly to the terminal CysSe492. For the bridging mechanism, this pathway cannot be used, but an alternative one going over His77, His430, and Tyr442 can be used instead.

Most of the DFT studies performed agree on the general features of the heterolytic dihydrogen cleavage. The different proposals have been recently reviewed by Bruschi et al.[8] In one of the earliest studies, De Gioia et al.[81,82] suggested essentially the mechanism described above with the same intermediates. For the product of the H−H cleavage, the proton was assumed to go to the terminal cysteine on nickel. Niu et al.[86] were the first to optimize a transition state which led directly to the protonated terminal cysteine, like the one in Figure 4. Before that study, Pavlov et al.[83] obtained the alternative transition state, instead leading directly to a protonated bridging cysteinate. The latter two studies advocated an oxidized $Ni^{III}Fe^{II}$ active state for the dihydrogen cleavage. In the study by Niu et al.,[86] a different approach was used to identify plausible intermediates, using a correlation between calculated C−O distances and experimental IR frequencies for the CO ligand.

In a quite recent study, Pardo et al.[94] reinvestigated the catalytic cycle with particular emphasis on the participation of high-spin states. The analysis again used the IR frequencies of the CO ligand. It was concluded that the structures and IR frequencies of the high-spin states better fit observations than those of the low-spin states. The $Ni^{III}Fe^{II}$ state was found to be the active state. The largest differences between the results by Pardo et al. using a model of type A in Figure 2 and those described above using the larger B model involve the importance of high-spin Ni^{II} and the question of whether nickel is oxidized before dihydrogen cleavage.

A somewhat different mechanism was suggested by Stein and Lubitz.[95,96] Rather than a cysteine ligand, they advocated a water molecule as the acceptor for the proton based on an analysis of magnetic resonance parameters. The resulting H_3O^+ product should form hydrogen bonds to the cyanides. In the reactant, hydrogen was suggested to bind terminally to nickel in line with other suggestions based on experiments.[91,92] The active state for dihydrogen cleavage was Ni^{III}-Fe^{II}.

In the only QM/MM study of the intermediates of the catalytic cycle, Amara et al.[71] optimized structures believed from experiments to be involved in the cycle and compared them to available X-ray data. Even though the catalytic cycle

suggested from these calculations has similarities to the one described above, there is also a significant difference. It is suggested that a bridging hydride is present all the time during catalysis, and the hydride obtained after the heterolytic cleavage is therefore placed as a terminal ligand on nickel. Another difference is that the terminal Cys65 ligand is protonated in Ni_a-C*. The Ni^{I} or Ni^{III} oxidation state of this species should critically depend on the charge of the proton on Cys65.

2.2.2. Hydride Transfer

The product of the previous electron- and proton-transfer step is a $Ni^{III}Fe^{II}$ state with a bridging hydride. The distance between nickel and iron is quite short, 2.63 Å, in agreement with the short distance in the X-ray structure for the reduced state.[47] The reason for this is the presence of the bridging hydride. The question of whether a bridging hydride is needed to obtain such a short distance has been debated.[97] Optimizations of a variety of different NiFe complexes show that this is not strictly required.[69] A few complexes with short Ni−Fe distances were actually found which do not have bridging hydrides, but these complexes turned out to be poor models for any state of the hydrogenase catalytic cycle.

An interesting aspect of the bridging $Ni^{II}Fe^{II}$ hydride singlet structure concerns the direction of the weakly bonding axis on nickel.[69] With the hydride, there are five ligands around nickel, and one of these is therefore forced to be axial. Because the other four ligands should be in one plane, there is essentially only one possible axial ligand, and this is Cys495, which thus forms a longer Ni−S distance than the other ones, 2.79 Å compared to 2.30−2.34 Å. The hydrogen bond to His77 stabilizes this structure further. For the oxidized $Ni^{III}Fe^{II}$ state, this tendency is still there but less marked, with a Ni−S distance to Cys495 of 2.57 Å. It is interesting to note that the Ni−S distances of the X-ray structure of the reduced enzyme[47] actually show exactly the same distortion of the cysteine ligands (see Figure 1). The experimentally found distortion has led to the suggestion of a possible involvement of the nickel triplet state.[76,77] However, another possibility is thus that the distortion is due to the presence of a bridging hydride, which is too small to be seen in the X-ray structure. With the presence of the hydride, the structure is quite normal with a plane with four ligands with short distances and with one axial ligand with a longer distance.

The next step of the catalytic cycle is the only one where a redox reaction is involved (apart from the obvious electron transfers). The bridging hydride should move to one of the cysteines. Only one DFT study has considered this part of the reaction mechanism, and it will be described here.[69] There are again essentially only two possibilities, moving it to the terminal CysSe492 ligand or to the bridging Cys495 ligand. However, the barrier for the latter pathway was found to be prohibitively high, 25 kcal/mol. The transfer to the terminal Cys492 is much easier with a barrier of only 4.7 kcal/mol. The optimized transition state is shown in Figure 5. The reason for this difference is that with a transfer to Cys492 the coordination around nickel can stay essentially the same along the entire transfer because both the hydride and Cys492 are in the coordination plane with the strong bonds in the Jahn−Teller distorted structure. In contrast, for the transfer to Cys495, the hydride is forced out of this plane to the weakly coordinated position for the axial Cys495.

In the final step of the hydrogenase catalytic cycle, an electron and a proton should be removed from the complex

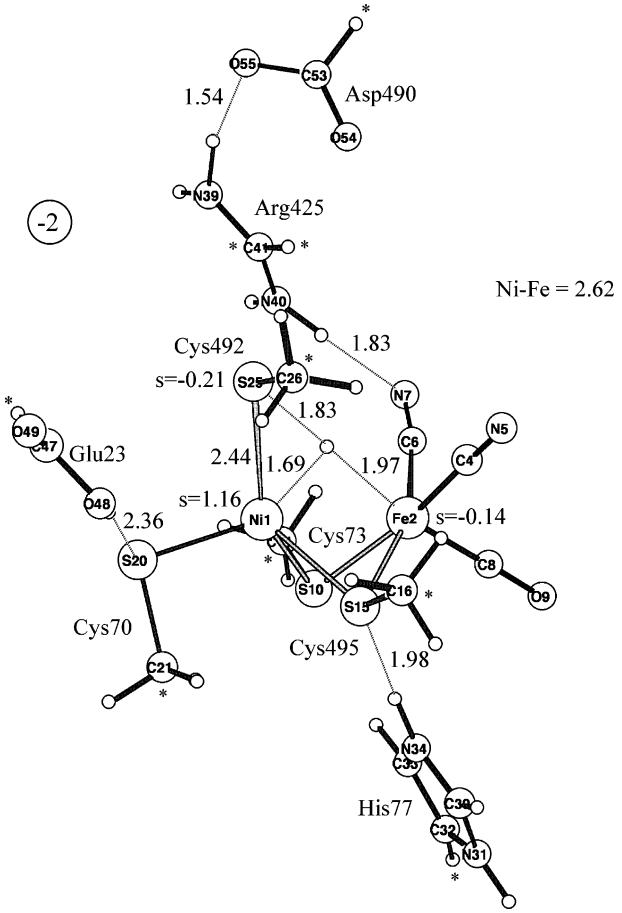

Figure 5. Optimized transition state for hydride transfer to Cys492 in Ni−Fe hydrogenase. The oxidation states are Ni^{I-III} and Fe^{II}. Distances in Å and spins larger than 0.1 are marked.

to return to the original reactant. The only DFT study considering this step uses the semiempirical procedure mentioned above.[69] As before, the combined energy of removing both of them at the same time was computed and found to be 62.3 kcal/mol. This is 3.0 kcal/mol more than for the first H^+,e^- removal, which should be used directly in the construction of the final energy diagram (see below). The pathways for electron and proton transfer should be the same as in the terminal pathway after the heterolytic cleavage of dihydrogen. The entire mechanism as discussed above is shown in Figure 6.

2.2.3. Constructing an Energy Diagram

In the calculations described above, the reaction barriers and energies for dihydrogen cleavage and hydride transfer have been obtained, as well as the energies for removing H^+,e^- twice leading back to the original reactant. Still, this is not enough to construct an energy diagram describing the catalytic cycle. So far, only one attempt has been made to present a full energetic cycle,[69] and in this case the semiempirical procedure mentioned above was used. In this approach, one single empirical parameter is used, and this is the total driving force for the full catalytic cycle. Alternatively, pK_a values and redox potentials for donors and acceptors have to be obtained in addition to the energies already calculated. As already mentioned, it is extremely difficult and tedious to obtain values of high accuracy for these quantities requiring the use of elaborate QM/MM models, and this has therefore so far not been done. The

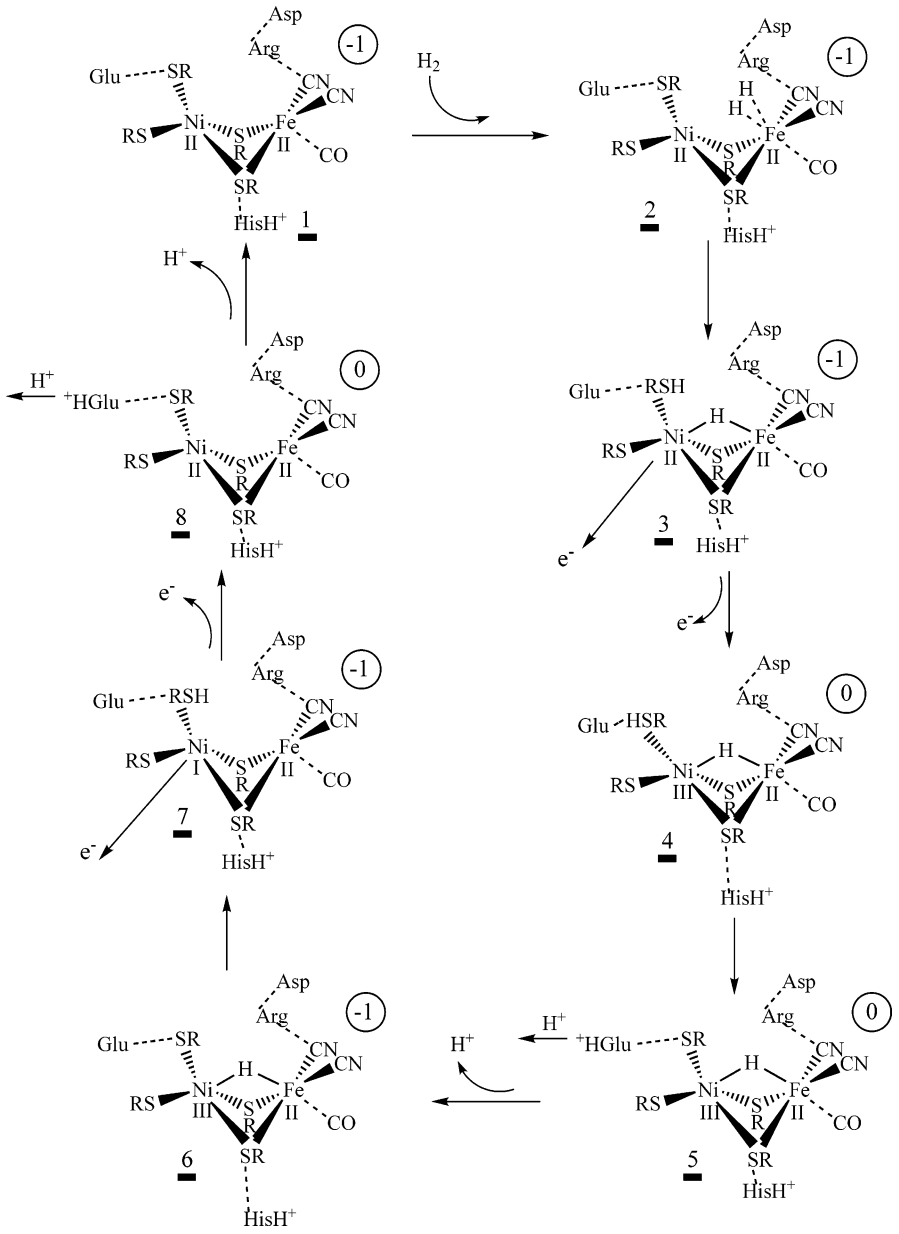

Figure 6. Suggested catalytic cycle for Ni−Fe hydrogenase.

main problem with the semiempirical approach is that the driving force is not known for hydrogenase. However, because the energy of the driving force is wasted as heat, the enzyme will try to minimize it, indicating that the driving force should be quite small. Also, hydrogenases are known to catalyze the reverse process of dihydrogen formation under certain circumstances, which is also an indication of a small forward driving force. In the construction of the energy diagram in Figure 7, a small value of −1.0 kcal/mol was therefore used. Choosing a value larger by a few kilocalories/mole would not change the energy diagram significantly. As seen in this energy diagram, most energy values were taken directly from the calculations, as described above. For the removal of the two H^+,e^-, values of 59.3 and 62.3 kcal/mol were calculated. The energy difference in these processes of 3.0 kcal/mol was used directly from these results, but the absolute values were adjusted to produce the desired driving force of −1.0 kcal/mol. This means that the first removal of H^+,e^- becomes exergonic by 1.5 kcal/mol, and the other one becomes endergonic by −1.5 kcal/mol because the energy difference of 3.0 kcal/mol has to be kept.

To identify the resting state of the cycle and the rate-limiting barrier, it is useful to consider two cycles after each other, as in Figure 8. The rate-limiting barrier is then easily identified as going from −4.1 kcal/mol in the first cycle to +11.6 kcal/mol in the second cycle, a barrier of 15.7 kcal/mol. This is the value that should be used in a comparison to experimental rate determinations. The experimental k_{cat} of 10^3 sec^{-1} [19] can be translated to a free energy barrier of around 13 kcal/mol by using transition state theory. The use of the B3LYP functional consequently overestimates the barrier by a few kilocalories/mole, which is common in bond-cleavage reactions.[98] If the internal barrier for dihydrogen cleavage of 12.6 kcal/mol is used for the rate determination instead, the concentration of the reactant **1** has to be taken into account. This concentration depends directly on the energy difference of +3.1 kcal/mol to the lowest energy before the barrier. Multiplying the concentration of **1** with the rate to go over a barrier of 12.6 kcal/mol leads exactly back to the result obtained by using the rate-limiting barrier of 15.7 kcal/mol without multiplying with any concentration. The resting state of the catalytic cycle in the energy diagram

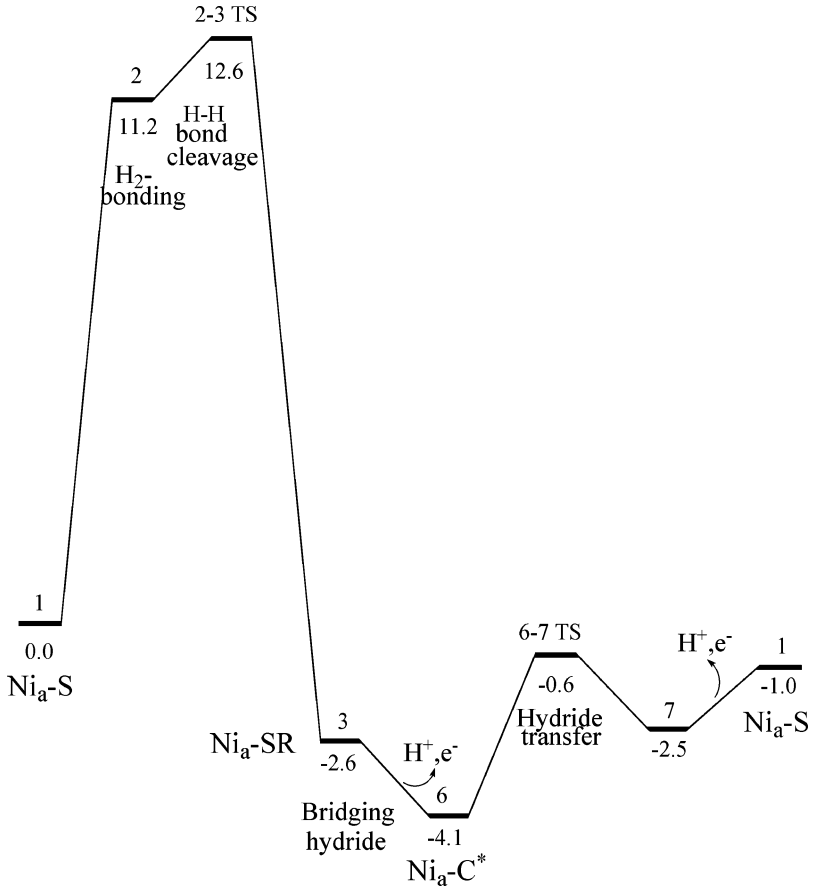

Figure 7. Energetics for the suggested catalytic cycle for Ni−Fe hydrogenase. The numbers for the structures are those from Figure 6.

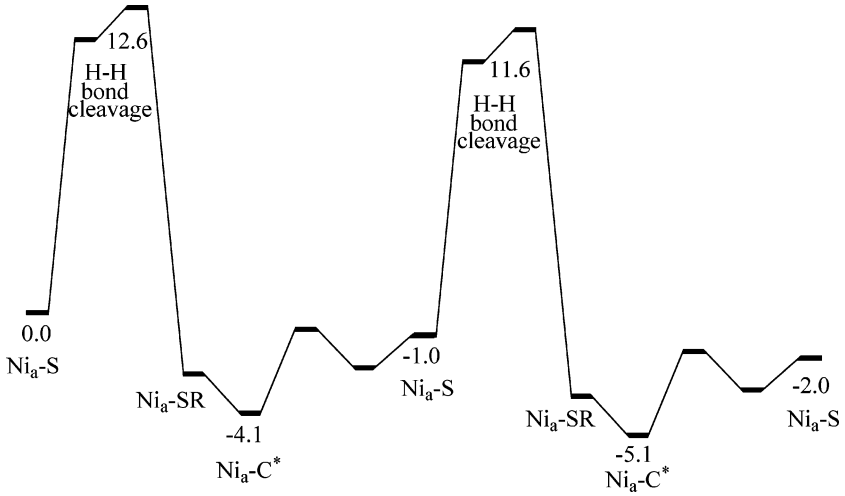

Figure 8. Energetics of two catalytic cycles for Ni−Fe hydrogenase.

is identified as Ni_a-C*, which is the state observed by X-ray crystallography for the reduced enzyme (see Figure 1). This is an EPR-active $Ni^{III}Fe^{II}$ state in line with spectroscopic information. The other two states observed under certain conditions in the catalytic cycle, Ni_a-S and Ni_a-SR, may also be tentatively assigned in the diagram as the immediate reactant and product of the dihydrogen cleavage, and both are $Ni^{II}Fe^{II}$ states as discussed above. Ni_a-SR would thus also have a bridging hydride like the Ni_a-C* state, whereas the Ni_a-S state would have an empty site in between nickel and iron, with neither a hydride nor a dihydrogen molecule.

The assignment of Ni_a-C* as a $Ni^{III}Fe^{II}$ state with a bridging hydride is in line with most suggestions based on DFT model calculations. In DFT studies of the mechanism for H_2 activation, this state came out as the most natural candidate for Ni_a-C*.[71,81,82,85,87] Hall and co-worker used a comparison of calculated and measured IR frequencies for the CO and CN ligands to make this assignment for Ni_a-C*.[86,88] They also suggested that one of the terminal cysteines is protonated. The presence of a bridging hydride was furthermore found to be consistent with EPR and IR data.[95,96,99,100] A comparison of the experimental g-tensor magnitudes and orientations showed good agreement with those predicted by DFT calculations for several models of the active site.

The diagrams shown in the figures contain the main information of present interest, allowing identification of the resting state and the other intermediates observed and also

the rate-limiting barrier. Still, some energies are missing for a complete picture, and these are the separate energies required to transfer first the electron and then the proton one at a time to the respective acceptors. To obtain these values, the individual energies to remove an electron and a proton from the NiFe complex must first be calculated. To remove an electron was found to cost 93 and 90 kcal/mol in the two cases, and for removing a proton, the cost was 282 and 288 kcal/mol (the electron was removed before the proton in each case). Again, to relate these values to energies in the diagram, a semiempirical scheme can be adopted requiring a single additional parameter. This parameter can be determined by minimizing the resulting barriers in the diagram, assuming that this is what has been achieved by the evolution of the enzyme. This has not been done in the case of hydrogenase but was used successfully for the respiratory enzyme cytochrome c oxidase[101] and for photosystem II,[102] and the reader is referred to these papers for details of the procedure.

Once an energy diagram like the one in Figure 7 had been constructed,[69] it was then possible to go back to the question of whether the $Ni^{II}Fe^{II}$ state is the active state, as assumed above, or if it could be the $Ni^{III}Fe^{II}$ state, as suggested in several early studies of the mechanism.[85,86] In these early studies, it was found that the dihydrogen cleavage is more exothermic for $Ni^{III}Fe^{II}$ which was considered an advantage, and this state was therefore preferred as the active state. Although a high exothermicity tends to make the dihydrogen cleavage easier, it is not necessarily an advantage if reversibility along a single pathway is a condition for a viable mechanism. The key energy difference for reversibility, as seen in the energy diagrams, is the energy difference between the TS and the product for the cleavage. In the energy diagrams discussed above, this energy difference is 15.2 kcal/mol. For the $Ni^{III}Fe^{II}$ state, this energy difference is 23.0 kcal/mol, which does not support reversibility of the reaction. The exergonicity of the dihydrogen cleavage was found to be 14.3 kcal/mol compared to 2.6 kcal/mol for the $Ni^{II}Fe^{II}$ state, in line with the trend in the early studies. The conclusion would then be that if the $Ni^{III}Fe^{II}$ state would be the active state in the cleavage reaction the reaction would not be reversible along the same pathway, which is the main argument against this active state. In contrast, Pardo et al.[94] argued that the forward and reverse reactions may follow different pathways, Thus, activation would involve electron loss first and then H_2 cleavage with Ni^{III}, but production would involve electron capture first and then H_2 formation on Ni^{II}. Such a hysteresis is possible only if conditions such as concentration and potential are significantly different in these two processes.

2.3. Oxidized States of [NiFe] Hydrogenases

Several theoretical studies investigating what happens when the [NiFe] cluster is oxidized have also been performed. A number of oxidized states have been observed experimentally. Reaction with dioxygen leads to the formation of the so-called unready state (Ni_u, or Ni-A) of the enzyme. This is a reaction of significant technological interest in the context of coupling hydrogen fuel production to the water splitting of photosynthesis. In this process, hydrogen molecule formation is complicated by the fact that the dioxygen waste product of photosynthesis is an inhibitor for most hydrogenases. When the Ni-A state has been formed as dioxygen has entered the active site, it takes several hours to restore the activity of the enzyme, which is why this state is termed unready. The second most interesting oxidized state of the NiFe complex is the so-called ready state (Ni_r, or Ni-B). Ni-B returns faster to the active state, on the time scale of seconds, and it has therefore been termed ready.

There are two recent X-ray crystallographic investigations of oxidized [NiFe] hydrogenases.[63,64] In the most recent one of these, the resolution is as high as 1.1 Å. Structures were obtained for both the Ni-A and Ni-B states. The two different structural analyses for the Ni-A and Ni-B states are in basic agreement. The Ni-B state is concluded to have a bridging single oxygen-containing ligand between nickel and iron which most likely is a hydroxide. The structure of the Ni-A state is interpreted to show a hydroperoxide in the bridging region. A very surprising aspect of this structure is that the peroxide has a side-on, bidentate, binding mode to nickel, quite unusual in biology. In both studies, there are also indications of cysteine ligand oxidation forming S=O bonds, more so in the structure of *Desulfovibrio vulgaris* (Miyazaki F)[64] than in *Desulfovibrio gigas*.[63]

The bidentate mode of binding the peroxide in Ni-A came as a major surprise. To our knowledge, this type of structure had not been suggested before, experimentally or computationally. This means that all DFT studies prior to the X-ray determination only considered incorrect structures. Four DFT studies have been performed after the new X-ray structures were determined,[72,103−105] three of them showing major modeling problems in describing Ni-A (the fourth study did not attempt any energetic preference of the structure). These modeling problems have already been mentioned above, and it was emphasized that before the discrepancies between the model results and experiment have been clarified it cannot be ruled out that the same problems appear also for the model results of the dihydrogen activation mechanism discussed above, which therefore at the present stage have to be taken with some caution. The description of the oxidized states will here start with the most recent study, which is also the one that uses the by far largest model with nearly 120 atoms.[105] This should not be interpreted to suggest that this particular study gives correct results. On the contrary, it will be shown that this study, as well as the other ones recently performed, shows major discrepancies to experiments. Due to the modeling problems for Ni-A, the description will start with Ni-B because the results are much less controversial in this case with nearly full agreement with experimental interpretations.

2.3.1. Ni-B

For the first X-ray structure of Ni-B that became available about a decade ago,[57] the oxygen-containing ligand bridging iron and nickel was tentatively suggested to be a μ-oxo ligand. In an early DFT study, Stein and Lubitz confirmed the bridging μ-oxo ligand in Ni-B based on comparisons of calculated and measured EPR spectra.[106] However, the first hybrid DFT studies instead indicated that this ligand most probably is a hydroxide.[84,86] With a hydroxide, the decrease of the Ni−Fe distance for the bridging hydride structure of Ni_a-C* compared to Ni-B was nearly perfectly reproduced by the calculations.[84] Most recent studies, experimental and theoretical, now agree that the bridging ligand is a hydroxide[63,64,72,94,107]

A schematic structure for the Ni-B doublet state is shown in Figure 9. The optimized geometries of the smallest models are very similar to those of the largest one.[105] Although there are some minor discrepancies, the overall structure is in good

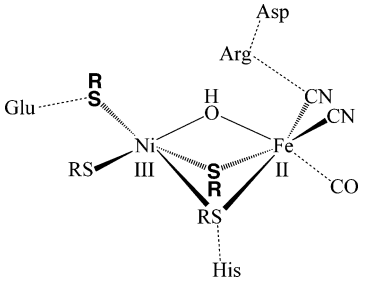

Figure 9. Schematic structure of Ni-B.

agreement with structure 1YRQ of the X-ray analysis.[63] The discrepancies show the normal pattern for medium basis QM models.[108,109] Covalent and ionic bonds are too long, and hydrogen bonds are too short. Some of the discrepancies to the Ni-B structure of *Desulfovibrio vulgaris* (Miyazaki F)[64] are larger. For example, the Ni−O distance of that structure is only 1.67 Å, which is significantly shorter than what is obtained in DFT optimizations of around 1.9 Å. The very short Ni−O distance of 1.67 Å indicates some double bond character not seen in the model calculations. This result could perhaps suggest that the bridging oxygen-derived ligand is not protonated for this species.

The most careful theoretical analysis of the structures of the oxidized states of [NiFe] hydrogenase has been made by Ryde and co-workers.[72] They used a combination of quantum refinement and QM/MM methods and applied it to the X-ray density of one of the most recent crystals.[63] They found that the electronic density of the crystals, which contain several states, is best explained as a slow-equilibrium mixture of structures with a bound peroxide and structures with oxidized Cys residues. The QM/MM optimizations and accurate energy calculations clearly showed that structures with a bridging hydroxide in Ni-B are appreciably more stable than those with a bridging μ-oxo or water ligand, in line with most recent DFT studies of Ni-B. They also concluded that because the crystal structure shows clear signs of X-ray induced radiation damage, it is likely that also the active site has been partly reduced during data collection.

Ni-B is activated for the hydrogenase catalytic cycle by removing the bridging hydroxide. Two different pathways have been experimentally suggested for this activation.[63,110−112] One pathway activates Ni-B without additional electrons and is suggested to involve a hydrogen molecule. A schematic picture of the two most likely types of transition states for this activation is shown in Figure 10. An approximate transition state of the first type, with the hydroxide on nickel, led to a computed barrier of 19.4 kcal/mol using B3LYP with a rather large model of type Figure 2B,[105] which is in line with an activation of Ni-B within seconds.[63] In a recent study by Jayapal et al.,[103] a somewhat lower barrier of 15.1 kcal/mol was obtained. This difference is expected because they used the nonhybrid BP86 method which is known to yield lower barriers than B3LYP. Another difference is that the hydroxide is pushed to the iron site in their TS (the second type in Figure 10) rather than to the nickel site as in the TS for the B3LYP model calculations. Both types of TSs were tested for the larger model using B3LYP, but the one with hydroxide on nickel was found to be significantly lower, probably due to the interaction between the hydroxide on iron and Arg476, not included in the calculations by Jayapal et al., who used a model like the one in Figure 2A.

The second pathway suggested experimentally involves activation of Ni-B by adding an additional electron and proton. An optimized TS of the type shown in Figure 11

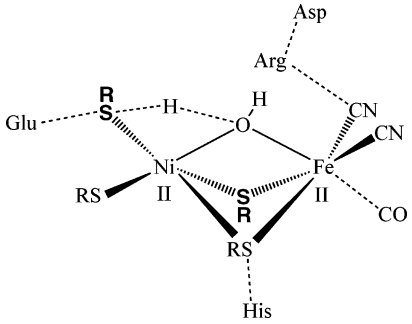

Figure 11. Schematic structure of the triplet transition state for the activation of Ni-B with one electron and one proton.

has been optimized for the medium size model.[105] The computed barrier was 19.2 kcal/mol, very close to the barrier for the other activation mechanism and a rate in reasonable agreement with the experimentally observed activation in seconds. It should be added that quite large distortions of the experimental structure were found in the B3LYP optimizations for both these types of activations of Ni-B, which means that the results have to be taken with some caution at present.

2.3.2. Ni-A

The suggestions for the bridging ligand in Ni-A have differed much more than the ones for Ni-B. By comparing the energy-minimized geometry with the crystal structure, De Gioia et al. suggested a μ-oxo ligand.[81,82] Amara et al. proposed a similar model.[71] Li et al. instead proposed a μ-OH ligand and that one terminal sulfur is protonated.[88] On the basis of the best fit to r_{CO}/ν_{CO} for synthetic compounds, where r_{CO} is the calculated C−O bond length and ν_{CO} is the experimental IR frequency, Fan et al. also suggest a μ-OH ligand.[87] Stadler et al. considered nine possible candidates for Ni-A and Ni-B by using calculated and measured magnetic resonance parameters and concluded that both these oxidized states probably have a μ-OH ligand. A peroxide

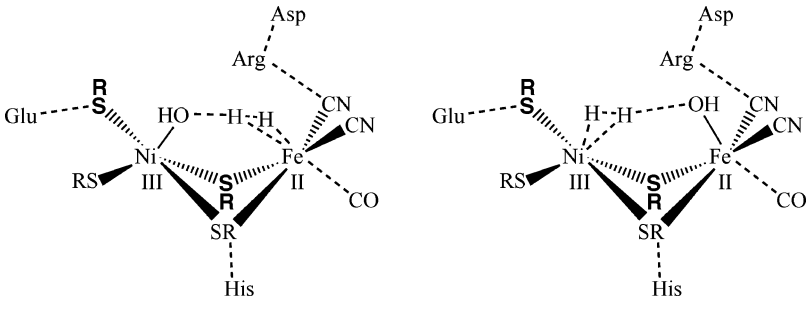

Figure 10. Schematic structures for the two alternative doublet transition states for the reaction between Ni-B and a hydrogen molecule.

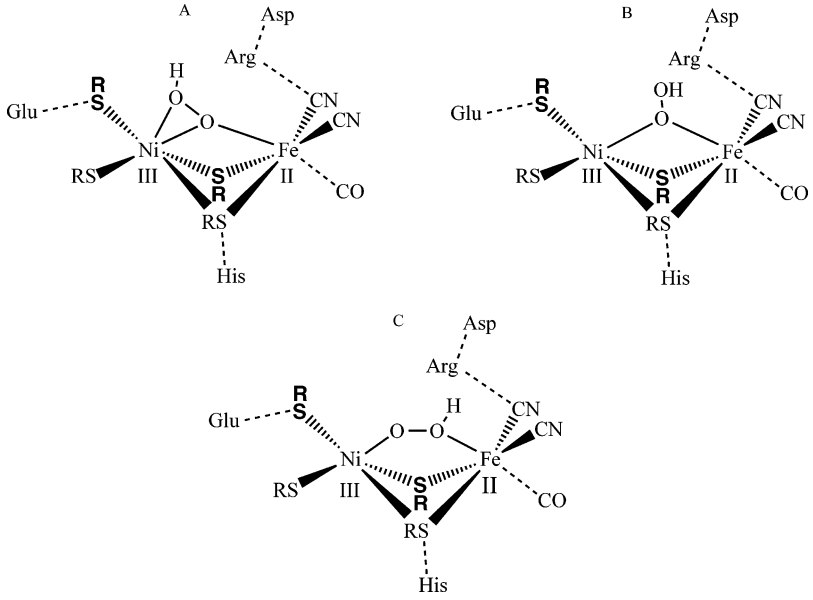

Figure 12. Three alternative structures obtained for Ni-A.

was not considered. It was suggested that the difference between the states could instead come from different protonations of the terminal cysteines.[107] By comparing calculated and measured g-tensors, Stein and Lubitz[95] tried to identify the bridging ligand in Ni-A. However, the calculated results were in poor agreement with experiments for the bridging μ-OH and μ-oxo ligands, which were the only ones considered. A bridging peroxide was not attempted. In a quite recent DFT study,[113] after the bridging peroxide had been suggested,[111] van Gastel et al. concluded that the bridging ligand is different in Ni-A and Ni-B based on a comparison of computed and measured ENDOR parameters, but a full characterization of the bridging ligand could not be made. Most of the early investigations thus indicated a bridging hydroxide for both Ni-A and Ni-B. However, after the recent reanalysis of the X-ray structures[63,64] including a high-resolution (1.1 Å) structure, it must now be almost established that the bridging ligand is a peroxide in Ni-A.

As already indicated, theoretical studies of Ni-A have been hampered by serious modeling problems even after the correct bridging peroxide structure was established experimentally. In the most recent study,[105] a structure very similar to the ones observed experimentally, like structure A in Figure 12, was finally found after a large number of attempts using the largest model shown in Figure 2C. As in the experimental structures, the protonated peroxide is bound side-on to nickel. There is a hydrogen bond to Arg476 holding it in place. The critical peroxide to metal distances are all reasonably well reproduced by the calculations. The Ni−O distances are both 2.05 Å, whereas they are 1.90 and 2.11 Å experimentally.[63] Again, the discrepancy compared to the *Desulfovibrio vulgaris* (Miyazaki F)[64] is larger. The short Ni−O distance reported for this structure is only 1.70 Å. It is not possible to explain the extremely short Ni−O distance by a possibly unprotonated peroxide for this species because removing the proton (and an electron) makes the Ni−O distances still longer in the model calculations. The computed Ni−Fe distance of 3.0 Å is in reasonable agreement with the experimental values of 2.93[63] and 2.80 Å,[64] as is the Fe−O distance of 2.09 Å compared to 1.90[63] and 2.20 Å.[64] Overall, it is clear that this computed structure corresponds to the one observed experimentally. It should in this context be emphasized that no constraint was put on the Ni−O distances in the calculations.

The problem of modeling Ni-A does not concern structure A in Figure 12 but the tendency for the optimization to reach structure B in the same figure instead. This structure turns out to be as much as 13.7 kcal/mol more stable than structure A at the B3LYP level, which is clearly a severe discrepancy compared to experiments. The same problem has been noted also in the other recent DFT studies.[103,104] The difference of 13.7 kcal/mol can be decomposed into different contributions. With the small lacvp basis set used for the geometry optimization, the difference was found to be only 2.2 kcal/mol. The large cc-pvtz(-f) basis set increased the difference to 9.6 kcal/mol, and the differential dielectric effects of 4.1 kcal/mol led to the final difference of 13.7 kcal/mol. The first suspicion of where the problem might be concerned the use of the B3LYP functional. The most critical parameter in B3LYP is the amount of exact exchange. Varying the amount of exact exchange is therefore a useful test to get an indication of the reliability of a B3LYP result. In all cases with significant discrepancies between B3LYP and experiments detected so far (an error of more than 5 kcal/mol), the results with nonhybrid methods (without exact exchange) have thus turned out to give results significantly different from B3LYP. No counterexample of this rule of thumb has so far been found. In the present case, the results using the nonhybrid methods BP86 and BLYP gave results quite similar to the ones using B3LYP. The energy difference between the two structures was found to be 13.0 kcal/mol at the BP86 level and 17.2 kcal/mol at the BLYP level. Following the normal rule of thumb, the conclusion was that the B3LYP result should be quite reliable in this case.

Many alternative structures for the peroxide in Ni-A were tried in the recent study.[105] The best one of these is shown as structure C in Figure 12. This structure was in fact found to be very similar in energy, within 1 kcal/mol, to the best of the peroxide structures, structure B, and is thus nearly 14 kcal/mol more stable than the structure observed experimentally, structure A.

Assuming that the tests described above indicate that there is no problem in this case to describe Ni-A using the B3LYP functional, the most likely explanation for the error at first

appeared to be that the chemical model used is not adequate for some reason. Maybe, with a still larger model, some enzyme interaction will severely limit the stability of structure B (and C) in Figure 12. However, it appears that the main destabilizing interactions from the enzyme should already be included in the large QM model. Another possibility is that van der Waals interactions, not included in DFT, and electrostatics from groups far away have a large differential effect. Investigations comparing QM/MM with even larger QM models are presently performed to investigate these possibilities, but so far only minor effects of the enzyme surrounding have been found. Instead, the protonation states of the cysteines appear to be critical, but this investigation is still in progress.

As already mentioned above for Ni-B, the most careful theoretical analysis of the structures of the oxidized states of [NiFe] hydrogenase has been made by Ryde and coworkers.[72] From the analysis of the electron density, they conclude that a peroxide ligand may exist as a minor component in the crystal. Their QM/MM calculations show that the structure suggested experimentally with a peroxide is chemically reasonable, and they conclude that it is therefore possible that the reported structures contain a peroxide ligand. However, even though the protein preparation contains a mixture of states with as much as 80% Ni-A, the quantum refinements indicated that a hydroxide bridge fitted the electron density map better, although they could not exclude that peroxide structures are present as minor conformations in the crystal. The reason for that was suggested to be that the active site has been photoreduced by X-ray radiation. Still, with a resolution as high as 1.1 Å in the most recent X-ray study,[64] the assignment of the bridging peroxide appears to be without question.

A remaining complication in the comparison between experiments and calculations is that the experiments also suggest substantial oxidations of the cysteine ligands, both terminal and bridging. However, these oxidations appear to be only fractional, and to what extent the oxidations could affect the final structure is therefore not clear at the present stage. Recent calculations by Pardo et al. suggest that these hydroxo/sulfenate forms are quite stable, and they have g values and CO stretching frequencies similar to the hydroperoxo forms.[94] Future studies of QM/MM type could probably resolve these issues.

In the only DFT study of the activation of the bidentate peroxide form of Ni-A performed so far,[105] it was assumed that some important interaction is missing even in the largest model used of type Figure 2C, which if included would prevent the formation of structure Figure 2B (and C).[105] It was also assumed that model Figure 2C is capable of adequately describing structure A. The activation of structure A of Ni-A turned out to be quite different from the one of Ni-B. If a proton (and an electron) is transferred to the NiFe complex, with the added proton going to the unprotonated oxygen of the peroxide, the O−O bond of the peroxide is cleaved without any barrier. The barrier for transferring the proton to this position was not calculated. A schematic picture of the product structure is shown in Figure 13. This structure, which has one hydroxide in between nickel and iron and one terminal hydroxide on nickel, was found to be 46 kcal/mol more stable than H_2O_2 bound in between nickel and iron. The electronic structure of this state can be described as Ni^{II}-triplet, coupled to Fe^{III}-doublet, coupled to a sulfur radical delocalized on Cys72 and Cys543. To remove

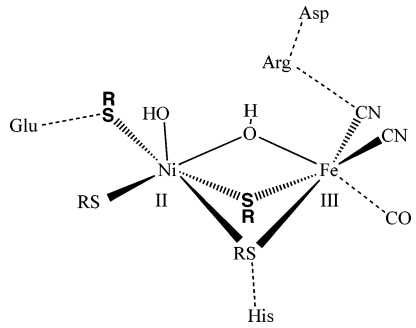

Figure 13. Schematic structure for the triplet product after the dissociation of the O−O bond. One electron and one proton have been added to Ni-A.

the two hydroxides to activate the enzyme would require two additional electrons and protons. All together, starting with the experimental structure A of Ni-A, three outside electrons and three protons would thus be required to activate the enzyme. This should be compared to the activation of Ni-B which only requires one outside electron and one proton and which can even be activated without outside electrons if a hydrogen molecule is used. These scenarios could be the reason Ni-A is so much harder to activate than Ni-B. However, additional calculations using QM/MM models would be required to substantiate these suggestions. Another indication that the scenario described here could be correct is the fact that adding CO actually helps to activate Ni-A.[110−112] CO would then add at the empty terminal coordination site of nickel and could perhaps prevent the formation of structure A of Ni-A, which requires two empty coordination sites on nickel.

3. [FeFe] Hydrogenases

3.1. Biochemical Studies on [FeFe] Hydrogenases

The second major class of hydrogenases is iron−iron hydrogenases ([FeFe]H_2ases).[80,114,115] Although the [NiFe]-H_2ases are generally found to catalyze H_2 oxidation, the [FeFe]H_2ases generally catalyze proton reduction. Nevertheless, H_2-oxidizing and bidirectional [FeFe]H_2ases are also known. Molecular structures have been derived from the X-ray crystallographic analysis of the H_2 uptake [FeFe]H_2-ase derived from *Desulfovibrio desulfuricans* Hildenborough (DdH) and the H_2-producing [FeFe]H_2ase derived from *Clostridium pasteurianum I* (CpI) (see Figure 14).[116−119] Although these [FeFe]H_2ases were derived from different sources and under different crystallization conditions, they have many structural similarities.[49,116−119] These [FeFe]H_2-ases both feature an unusual 6-Fe active site cluster (known as the H-cluster or $[6\text{-Fe}]_H$). Analysis of their solid-state structures shows that the H-cluster is connected to the enzyme surface by a gas access channel, hydrogen-bonded proton-transfer pathways, and two ferrodoxin-like [4Fe-4S] clusters.[120]

The $[6\text{-Fe}]_H$ cluster consists of an unusual di-iron cluster (referred to as $[2\text{-Fe}]_H$, [FeFe], or the di-iron cluster) bridged to a typical [4Fe-4S] cluster by a protein-bound cysteine ligand.[49,116−119] The di-iron portion of the H-cluster is the putative site of H^+ reduction and H_2 oxidation (see Figure 15). Each iron atom of the di-iron cluster is further coordinated by one terminally bound CN and one terminally bound CO ligand. The two irons are bridged by a novel five-atom dithiolate bridge generally assigned as either 1,3-

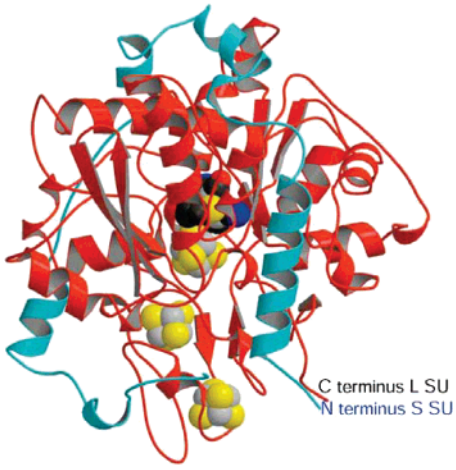

Figure 14. Representation of [FeFe]H_2ase enzyme derived from *Desulfovibrio desulfuricans* Hildenborough. The atoms of the H-cluster and [4Fe-4S] clusters are shown as spheres. The remainder of the protein is shown as a ribbon. Figure was reproduced from ref 118 with permission from Elsevier.

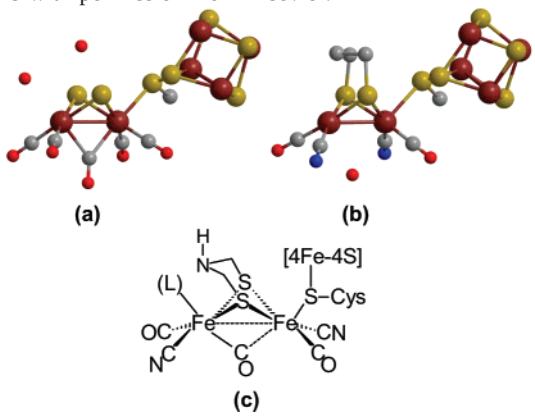

Figure 15. Structure of the active site of [FeFe]H_2ase. Original active site structures proposed by Peters et al.[116] and Nicolet et al.[118] for the [FeFe]H_2ase derived from CpI (a) and DdH (b), respectively. Concensus structure for the active site of [FeFe]H_2-ase (c). L = vacant, H_2O, OH^-, H^-, or H_2.

propanedithiolate (PDT, $-SCH_2CH_2CH_2S-$)[49] or 1,3-di-(thiomethyl)amine (DTMA, $-SCH_2NHCH_2S-$).[119] A third CO ligand is found either bridging the two iron atoms or terminally bound to the distal iron atom, apparently depending on the redox state of the di-iron cluster. (The two iron centers are commonly designated as proximal and distal by noting their spatial relation to the nearby [4Fe-4S] cluster and protein backbone.) Incubation of the active enzyme with CO gas results in the binding of an additional CO ligand to the distal iron to yield an inactive, CO-inhibited form of the enzyme.[117]

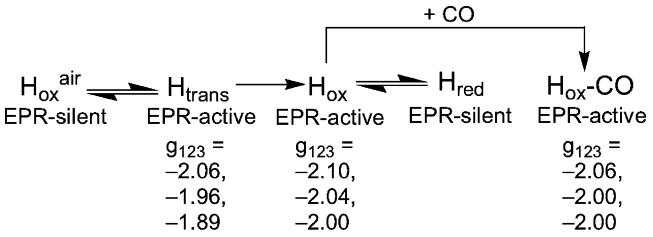

Figure 16. Summary of the EPR data from Albracht et al.[128] on the [FeFe]H_2ase derived from DdH.

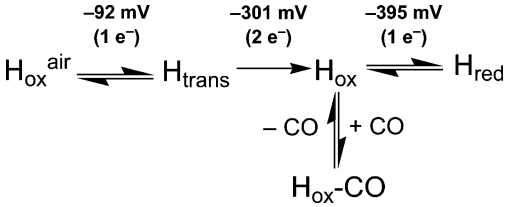

Figure 17. Summary of the infrared spectrochemical study of Roseboom et al.[128] Midpoint reduction potentials are at pH 8. The number of electrons transferred at each potential is given in parentheses.

Electron paramagnetic resonance (EPR)[121−124] and infrared (IR) spectral studies[119,125−127] have identified at least five forms of the [6-Fe]H cluster in the [FeFe]H_2ase derived from DdH. EPR and IR data are given in Figure 16 (summary of EPR data) and Table 3 (summary of IR data), respectively. The aerobic purification of the [FeFe]H_2ase derived from DdH results in a stable "overoxidized'', catalytically inactive form (labeled as $H_{as-isolated}$, H_{inact}, or H_{ox}^{air}) that is EPR-silent. Reduction of the H_{ox}^{air} form yields a transiently stable, EPR-active ($S = 1/2$) form referred to as H_{trans}. Prolonged reduction of H_{ox}^{air}/H_{trans} leads to a stable EPR-active ($S = 1/2$), active form (the so-called oxidized, active form) of the H-cluster that is referred to as H_{ox}. The application of more reducing conditions results in the reduction of the H_{ox} form to a stable EPR-silent form referred to as H_{red}. The addition of CO gas to the H_{ox} form yields a stable, catalytically inactive, CO-inhibited, EPR-active ($S = 1/2$) form known as $H_{ox}-CO$. The [FeFe]H_2ase from CpI is purified under anaerobic, reducing conditions, and only the H_{ox} and $H_{ox}-CO$ forms have been observed.[116,117]

Electrochemical conversions between these various forms were recently re-examined using infrared spectroelectrochemistry (see Figure 17).[128] (All of the midpoint potentials reported here for this study are at pH 8.) The H_{ox}^{air} form is converted to the H_{trans} form in a reversible one-electron reduction at −92 mV vs NHE. The H_{trans} form undergoes an irreversible two-electron reduction to yield the H_{ox} form at −301 mV vs NHE. In spite of this apparent two-electron reduction, the $[6\text{-Fe}]_H$ cluster does not appear to be reduced.

Table 3. Experimentally Determined ν(CO) and ν(CN) Bands for the [FeFe]H_2ase Enzyme Derived from DdH

state	ν(CO)	ν(CO)	ν(CO)	ν(CO)	ν(CX)[a]	ν(CN)	ν(CN)	ref
H_{ox}^{air} [b]		2007	1983	1847		2107	2087	119,125
H_{trans} [c]	1992	1982	1976	1835		2100	2075	128
H_{ox} [d]		1965	1940	1802		2093	2079	119,126
H_{red} [e]	1965	1940	1916	1894	2041	2093	2079	119,125
$H_{ox}-{}^{13}CO$ [f]	1995	1963	1949	1812		2096	2089	126
$H_{ox}-{}^{12}CO$ [g]	2016	1972	1963	1811		2096	2089	125,126

[a] X=O or N. [b] As isolated, in air. [c] Transient species observed after electrochemical reduction of H_{ox}^{air} at −162 mV. [d] After electrochemical reduction of H_{ox}^{air} at −535 mV, then oxidation at −285 mV, or after reduction of H_{ox}^{air} with H_2, then oxidation by H_2 loss under argon. [e] After electrochemical reduction at −535 mV or reduction with H_2. [f] After reactivation with H_2, followed by ^{13}CO atmosphere. [g] After reactivation with H_2, followed by ^{12}CO atmosphere.

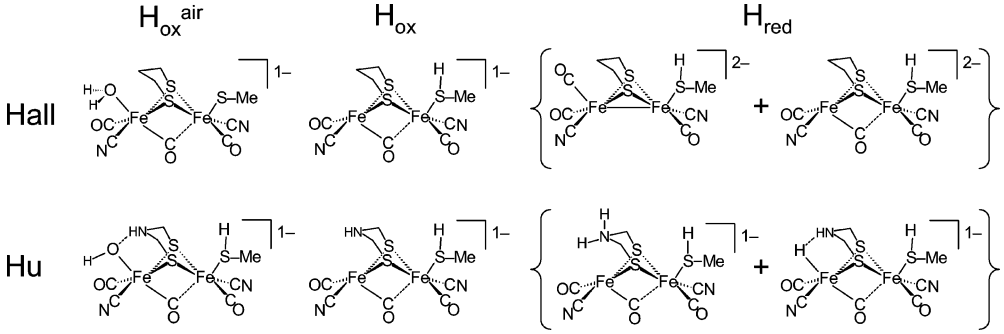

Figure 18. Computational models of Hall[134,139] and Hu[140,141] for which the computed ν(CO) and ν(CN) values most closely match the experimentally determined values for the H_{ox}^{air}, H_{ox}, and H_{red} forms of [FeFe]H_2ase. Subsequent works of Zilberman et al.[137] and Fiedler et al.[136] agree with the assignment of H_{ox} as an $Fe^{I}Fe^{II}$ form with an open site at the distal iron. However, Fiedler et al. conclude that inclusion of the proximal [4Fe4S] in the computations is necessary for a correct modeling of the EPR parameters.

The H_{ox} form undergoes a reversible one-electron reduction to the H_{red} form at −395 mV vs NHE. These results suggest that the oxidation level of the various forms of [FeFe]H_2ase decrease in the following order: H_{ox}^{air} (most oxidized form) > H_{trans} > H_{ox} > H_{red} (most reduced form).

Because the $[2\text{-Fe}]_H$ active site so closely resembles organometallic complexes such as $(\mu\text{-SEt})_2[Fe(CO)_3]_2$ and $(\mu\text{-SCH}_2CH_2CH_2S)[Fe(CO)_3]_2$, much experimental work has focused on modeling this hydrogenase. Initial experimental efforts focused on the synthesis and characterization of $[(\mu\text{-SCH}_2CH_2CH_2S)[Fe(CO)_2(CN)]_2]^{2-}$.[129] The IR spectra of these model complexes suggested that the oxidation states of the iron centers of the [FeFe]H_2ase enzyme were lower than those expected.[130]

3.2. DFT Calculations: Determining the Oxidation States of the H-Cluster

Mössbauer spectroscopy is generally the most powerful experimental tool for determining the oxidation state of iron atoms. For high-spin iron centers, the isomer shift is a very sensitive indicator of iron's oxidation state. For low-spin iron centers, however, the interpretation of the isomer shift in terms of an iron center's oxidation state is much more difficult. This fact leads to some ambiguity in the assignment of the oxidation state of the iron centers in the di-iron portion of the H-cluster.

Mössbauer[131−133] spectral studies have been performed on the [FeFe]H_2ases derived from several sources, but the results were compatible with more than one assignment of the oxidation states of the iron atoms in the various forms. Shortly after the publication of the molecular structure of the [FeFe]H_2ase from CpI, Münck and co-workers re-examined their earlier Mössbauer study on hydrogenase II derived from *Clostridium pasteurianum*.[131,132] They assigned the formal oxidation states of di-iron clusters as $Fe^{III}Fe^{II}$ for the H_{ox} and H_{ox}−CO forms and $Fe^{II}Fe^{II}$ for the H_{red} form. Pereira et al. used Mössbauer spectroscopy to examine an [FeFe]H_2ase derived from *Desulfovibrio vulgaris* (Hildenborough) and assigned the formal oxidation states of the di-iron cluster as follows: H_{ox}^{air} ($Fe^{III}Fe^{III}$); H_{trans} ($Fe^{III}Fe^{III}$); H_{ox} ($Fe^{II}Fe^{III}$); H_{ox}−CO ($Fe^{II}Fe^{III}$); H_{red} ($Fe^{II}Fe^{II}$). Both studies agree that the 4Fe-4S cluster should be assigned as the EPR-silent $[4Fe\text{-}4S]^{2+}$ in all of the active stable forms (the [4Fe-4S] cluster is EPR-active $[4Fe\text{-}4S]^{1+}$ in the H_{trans} form) and stated that the following assignments of the oxidation states are also consistent with the Mössbauer data: H_{ox}^{air} ($Fe^{II}Fe^{II}$); H_{trans} ($Fe^{II}Fe^{II}$); H_{ox} ($Fe^{I}Fe^{II}$); H_{ox}−CO ($Fe^{I}Fe^{II}$); H_{red} ($Fe^{I}Fe^{I}$).[131−133]

The iron(III) and iron(II) oxidation states are common in biological systems, but the presence of an iron center in the formal iron(I) oxidation was unprecedented. The synthesis and infrared spectral characterization of $[(\mu\text{-SCH}_2CH_2CH_2S)\text{-}[Fe(CO)_2(CN)]_2]^{2-}$, a synthetic complex that is structurally and compositionally similar to the di-iron portion of the [FeFe]H_2ase active site, lend credence to the oxidation state assignment of the H_{red} form as $Fe^{I}Fe^{I}$. Further synthetic model studies[130] suggest that the H_{ox}^{air}, H_{ox}, and H_{red} forms correspond, respectively, to $Fe^{II}Fe^{II}$, $Fe^{I}Fe^{II}$, and $Fe^{I}Fe^{I}$ formal redox states of the di-iron cluster.

In the first theoretical study of the stable species and cleavage reaction, Cao and Hall[134] used DFT calculations (B3LYP functional; DZP basis sets) to compute infrared stretching frequencies for a series of geometry-optimized structural candidates (the computational model was $[(L)(CO)(CN)Fe(\mu\text{-SCH}_2CH_2CH_2S)(\mu\text{-CO})Fe(CO)(CN)(L')]^q$ L = vacant, H_2O, CO, H_2, or H^-; L′ = CH_3S^- or CH_3SH; q = 0, 1−, 2−, or 3−) for the H_{ox}^{air}, H_{ox}, and H_{red} forms. (Infrared spectroscopy is another powerful tool for studying the [FeFe]-H_2ase active site as the iron-bound CO ligands are sensitive indicators of the electron density at the iron centers.[135]) They compared the experimentally determined and computed ν-(CO) and ν(CN) stretching frequencies for the $(\mu\text{-S(CH}_2)_3S)\text{-}[Fe(CO)_3]_2$ and $[(\mu\text{-S(CH}_2)_3S)[Fe(CO)_2(CN)]_2]^{2-}$ complexes to calibrate their computationally derived ν(CO) and ν(CN) stretching frequencies. Using this method, they were able to show that structural candidates with the $Fe^{III}Fe^{III}$ and $Fe^{II}\text{-}Fe^{III}$ oxidation states yielded computed ν(CO) and ν(CN) stretching frequencies that are systemically too high when compared to $H_{as-isolated}$ and H_{ox} forms. In addition, the computed infrared stretching frequencies were used to propose structural models for the various spectroscopically observed forms (summarized in Figure 18). For the H_{ox}^{air} form, the best structural candidate corresponded to an $Fe^{II}\text{-}Fe^{II}$ complex with a water molecule bound to the distal iron. For the H_{ox} form, the best structural candidate corresponded to an $Fe^{I}Fe^{II}$ complex with an open site on the distal iron. The H_{red} form was assigned to a mixture of two $Fe^{I}Fe^{I}$ structural candidates: (1) a structure with a bridging CO ligand and an open site on the distal iron and (2) a structure with all terminal CO ligands and an "open site'' between the two iron centers.

Liu and Hu[140,141] later performed DFT calculations (GGA-PW91; plane-wave basis sets) on a computational model with a slightly different S-to-S linker than used by Cao and Hall[134] ($\mu\text{-SCH}_2NHCH_2S$ rather than $\mu\text{-SCH}_2CH_2CH_2S$ to give $[(L)(CO)(CN)Fe(\mu\text{-SCH}_2N(H)xCH_2S)(\mu\text{-CO})Fe(CO)(CN)(CH_3\text{-}$

SH)]^q; L = vacant, H_2O, CO, H_2, H^-, OH, or O_2; $x = 1$ or 2; $q = 0$, 1−, or 2−). They compared the experimentally determined and computed ν(CO) stretching frequencies for the $[CpFe(CN)_2(CO)]^{1-}$, $CpFe(CNCH_3)(CN)(CO)$, $[Cp^*Fe(CN)_2(CO)]^{1-}$, and $CpFe(CN)(CO)_2$ (Cp = $[C_5H_5]^{1-}$, Cp* = $[C_5(CH_3)_5]^{1-}$) complexes to calibrate their computationally derived ν(CO) stretching frequencies. They also used their computed infrared stretching frequencies to propose structural models for the various spectroscopically observed forms (summarized in Figure 18). For the H_{ox}^{air} form, the best structural candidate corresponded to an $Fe^{II}Fe^{II}$ complex with OH^- bound to the distal iron. For the H_{ox} form, the best structural candidate corresponded to an $Fe^{I}Fe^{II}$ complex with an open site on the distal iron. A subsequent computational study by Fiedler and Brunold (BP86; triple-ζ basis sets and B3LYP; triple-ζ valence basis sets) confirmed the $Fe^{I}Fe^{II}$ nature of the H_{ox} and H_{ox}−CO forms and suggested that the inclusion of the proximal [4Fe4S] cluster is required for proper computation of the EPR parameters.[136] The H_{red} form was assigned to a mixture of two structural candidates: (1) an $Fe^{I}Fe^{I}$ structure with a bridging CO ligand and an open site on the distal iron and (2) one with the central amine of the S-to-S linker protonated and an $Fe^{II}Fe^{II}$ structure with a hydride ligand bound at the distal iron center.[140,141]

The experimental and theoretical studies presented above converge on the description of the forms of the $[FeFe]H_2$-ase active site. The H_{ox}^{air}, H_{ox}/H_{ox}−CO, and H_{red} forms correspond to the $Fe^{II}Fe^{II}$, $Fe^{I}Fe^{II}$, and $Fe^{I}Fe^{I}$ oxidation states. The H_{ox}^{air} form corresponds to an $Fe^{II}Fe^{II}$ redox level, and most likely H_2O or OH^- is strongly bound at the distal iron. Activation of the H_{ox}^{air} form probably involves removal of the bound H_2O or OH^- ligand by reduction of the di-iron cluster and/or protonation of the iron-bound OH^-. The H_{ox} form corresponds to a valence-localized $Fe^{I}Fe^{II}$ redox level with the unpaired electron residing mostly on the distal iron center. Water or no other ligand is closely bound at the distal iron center in the H_{ox} form. The H_{ox}−CO form corresponds to a valence-delocalized $Fe^{I}Fe^{II}$ form with an additional CO ligand bound to the distal iron center. A recent computational study (PBE functional; plane-wave basis sets) confirms the $Fe^{I}Fe^{II}$ oxidation state and the fact that the H_{ox}−CO form contains an additional CO ligand with respect to H_{ox}, but contests the generally accepted orientation of the CO and CN ligands about the distal iron center.[137] The H_{red} form corresponds to a mixture of at least two forms: one part corresponds to an $Fe^{I}Fe^{I}$ redox level with a semibridging CO, and the other part may correspond to either an $Fe^{I}Fe^{I}$ redox level with all terminal CO ligands or an $Fe^{II}Fe^{II}$ hydride complex.

3.3. DFT Calculations: Catalytic Mechanism for H_2 Oxidation/H^+ Reduction

DFT calculations have been applied by several research groups to give a better understanding of the molecular details of H_2 oxidation and H^+ reduction at the di-iron active site. The various proposed mechanisms differ mainly in the prospective location of H^+ and/or H_2 binding to the di-iron cluster (as shown in Figure 19). Hall, Hu, and respective co-workers[134,139−141] have examined the binding and cleavage of H_2 at the distal iron center. De Gioia, Zhou, and their respective co-workers examined the binding and cleavage of H_2 to the area "between'' the two iron centers.[142−145]

The seminal DFT study (BLYP functional; numerical basis sets) on the mechanism of H_2 cleavage was performed by

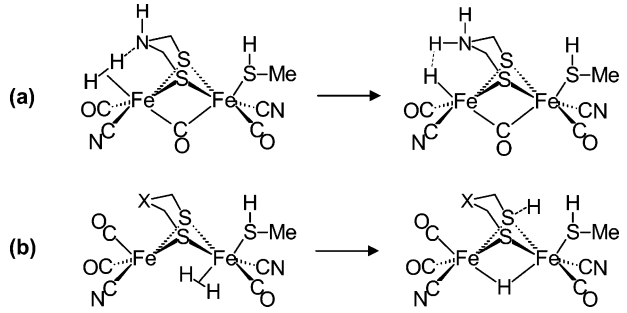

Figure 19. Heterolytic cleavage of H_2 using small molecule computational models of the $[FeFe]H_2$ase active site. Hall, Hu, and their respective co-workers (a) favor heterolytic cleavage of H_2 bound to the distal iron center and utilizing the central nitrogen of the S-to-S linker as an internal base.[134,139−141] De Gioia, Zhou, and their respective co-workers (b) favor heterolytic cleavage of H_2 bound to the proximal iron and utilizing a bridging thiolate sulfur atom as an internal base.[142−145]

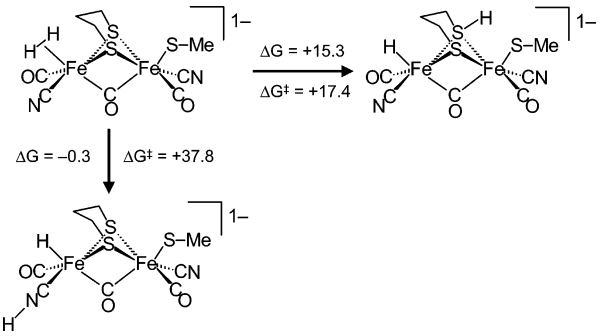

Figure 20. Cleavage of the H−H bond without the μ-SCH_2NHCH_2S linker or an external base. A proton is transferred from the η_2-H_2 ligand to a sulfur of the dithiolate linker or to the cyanide ligand attached to the distal iron. Computed changes in free energy (ΔG) and free energy barriers (ΔG) in kilocalories/mole reported by Cao and Hall.[134]

Dance[138] using the computational model $[(L)(CO)(CN)Fe(\mu_2\text{-}S_2)(\mu\text{-}CO)Fe(CO)(CN)(CH_3S)]^q$ (where L = vacant, H_2O, H_2, or H^-; μ_2-S_2 = $[S\text{-}S]^{2-}$ or $([\mu\text{-}S]^{2-})_2$; $q = 0$, 1−, or 2−) as suggested by the initial X-ray structure of Peters and co-workers.[116] Subsequent experimental work has suggested that the bridging sulfur atoms of the di-iron cluster are provided by a bridging dithiolate (i.e., μ-SCH_2XCH_2S) and not $[S\text{-}S]^{2-}$ or $([\mu\text{-}S]^{2-})_2$ as originally suggested.

The initial work of Cao and Hall[134] (B3LYP functional; DZP basis sets) used a computational model of the [FeFe]-H_2ase active site based on a revised structure of the [FeFe]-H_2ase active site with an all-carbon S-to-S linker (i.e., μ-$SCH_2CH_2CH_2S$) as suggested by Nicolet et al.[118] and focused on the binding and cleavage of H_2 at the distal iron. Using this model, they investigated two pathways leading to H−H cleavage (see Figure 20). Transfer of H^+ from η_2-H_2 bound at the distal iron of the $Fe^{II}Fe^{II}$ form to one of the bridging sulfur atoms was thermodynamically unfavorable (ΔG = +15.3 kcal/mol) but kinetically favorable (ΔG = +17.4 kcal/mol), whereas transfer of H^+ from η_2-H_2 bound at the distal iron of the $Fe^{II}Fe^{II}$ form to the nitrogen of the cyanide ligand bound to the distal iron was thermodynamically favorable (ΔG = −0.3 kcal/mol) but kinetically unfavorable (ΔG = +37.8 kcal/mol). Interestingly, they also found that an $Fe^{II}Fe^{II}$ complex with a bridging hydride ligand and terminal CO ligand is significantly more stable the constitutional isomer with a bridging CO ligand and terminal hydride ligand.[134]

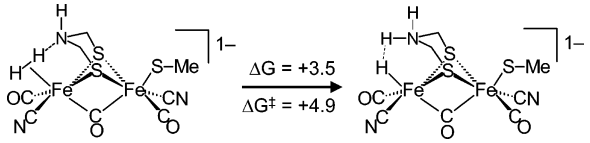

Figure 21. Cleavage of the H−H bond with the μ-SCH_2NHCH_2S linker. A proton is transferred from the η_2-H_2 ligand to the nitrogen atom of the dithiolate linker. Computed changes in free energy (ΔG) and free energy barriers (ΔG) in kilocalories/mole reported by Fan and Hall.[139]

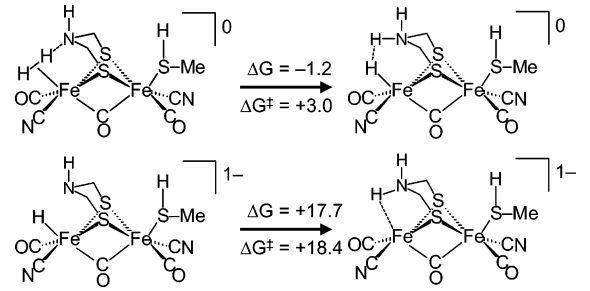

Figure 22. Cleavage of the H−H and Fe−H bond with the μ-SCH_2NHCH_2S linker. A proton is transferred from the η_2-H_2 and H^- ligands to the nitrogen atom of the dithiolate linker. Computed changes in free energy (ΔG) and free energy barriers (ΔG) in kilocalories/mole reported by Liu and Hu.[140,141]

Upon re-examination of the [FeFe]H_2ase structures, Nicolet et al. reassigned the S-to-S linker as μ-SCH_2NHCH_2S and identified a possible hydrogen-bonded proton-transfer pathway leading from the central nitrogen atom to the protein surface.[119] Hall and Fan[139] used DFT calculations (B3LYP functional; DZP basis sets) to examine the cleavage of H_2 bound at the distal iron center using the bridgehead amine of this S-to-S linker (see Figure 21). Transfer of H^+ from η_2-H_2 bound at the distal iron of the $Fe^{II}Fe^{II}$ form to the bridgehead amine was found to be kinetically and thermodynamically favorable ($\Delta G = +3.5$ kcal/mol; $\Delta G = +4.9$ kcal/mol).

Liu and Hu[140,141] also used DFT calculations (GGA-PW91; plane-wave basis sets) to examine H_2 oxidation at the distal iron center employing the μ-SCH_2NHCH_2S bridge (see Figure 22). They found that transfer of H^+ from η_2-H_2 bound at the distal iron of the $Fe^{II}Fe^{II}$ form to the bridgehead amine of the μ-SCH_2NHCH_2S appears kinetically and thermodynamically favorable ($\Delta G = -1.2$ kcal/mol; $\Delta G = +3.0$ kcal/mol). Interestingly, the transfer of the second H^+ from the terminal hydride species ($H-Fe^{II}Fe^{II}$) to yield fully reduced $Fe^{I}Fe^{I}$ species is kinetically and thermodynamically unfavorable ($\Delta G = +17.7$ kcal/mol; $\Delta G = +18.4$ kcal/mol). A kinetically and thermodynamically favorable route was found for transferring H^+ to NH_3, which serves as a model of the nearby lysine residue ($\Delta G = +4.2$ kcal/mol; $\Delta G = +6.5$ kcal/mol). This final result is unexpected because it would suggest that NH_3 is more basic than the secondary amine of the S-to-S linker. This unexpectedly large difference may be due to hydrogen bonding involving the transferred H^+ and the two nearby nitrogen bases.

De Gioia and co-workers[143−145] have examined an alternative pathway for H−H cleavage (Figure 23). In the De Gioia mechanism, the enzyme active site rearranges from the μ-CO structural form observed in the molecular structures of the [FeFe]H_2ase to a structural form with all terminal CO ligands creating an open site "between'' the two iron centers. Dihydrogen binds to one of the irons in this open site, and a proton is transferred from the bound η_2-H_2 to a μ-S atom

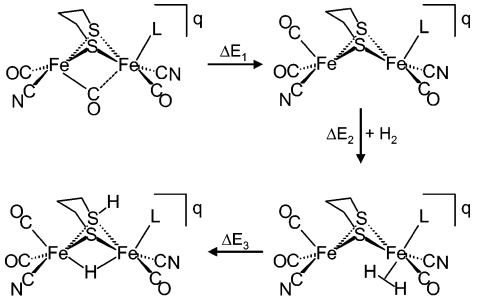

Redox Level of Irons	q	L	ΔE_1	ΔE_2	ΔE_3
$Fe^{II}Fe^{II}$	1–	MeS^-	–0.6	–15.3	2.4
$Fe^{I}Fe^{II}$	1–	MeSH	–0.9	–12.8	9.3
$Fe^{I}Fe^{II}$	2–	MeS^-	3.6	1.0	2.6

Figure 23. Binding and cleavage of dihydrogen on the proximal iron. In this mechanism, the ν(CO) structure of the [FeFe]H_2ase active site rearranges to a structure with all-terminal CO ligands. Dihydrogen binds to the proximal iron, and a proton is transferred to a sulfur of the dithiolate bridge. Computed changes in electronic energy $\Delta(E)$ in kilocalories/mole reported by De Gioia and co-workers.[143−145]

of the dithiolate bridge to yield a bridging hydride species. They compute (B3LYP functional; DZP basis sets) that rearrangement of the μ-CO form to the all terminal CO form is exothermic, −0.6 kcal/mol, for the $Fe^{II}Fe^{II}$ form using MeS^- as a model for the S-Cys[4Fe-4S] portion of the enzyme. The binding of H_2 to the proximal iron is exothermic by −15.3 kcal/mol. In the H−H cleavage reaction, the transfer of H^+ from the bound η_2-H_2 to one of the S atoms of the dithiolate is only endothermic by +2.4 kcal/mol. Using a model at the $Fe^{I}Fe^{II}$ redox level, with MeS^- they computed values of +3.6, +1.0, and +2.6 kcal/mol, respectively, for the μ-CO to all-terminal CO rearrangement, H_2 binding, and H−H cleavage, whereas using a model at the $Fe^{I}Fe^{II}$ redox level, with MeSH they computed values of −0.9, −12.8, and +9.3 kcal/mol, respectively, for the μ-CO to all-terminal CO rearrangement, H_2 binding, and H−H cleavage. The large changes in H_2 binding energies, −15.3 to +1.0 and back to −12.8, are in part due to the differences in the gas-phase ion-induced dipole forces.

De Gioia and co-workers examined the effects of a continuum solvation model (conductor-like screening model or COSMO) on the computed energetics (BP86; TZVP basis sets) of H_2 activation at the distal iron center and at the proximal iron center in the area between the two iron centers.[145] The bridging hydride/all-terminal CO species are consistently found to be more stable than the terminal hydride/bridging CO species both in the gas phase and after incorporating solvation effects. They calculate the change in free energy for transfer of H^+ from cleavage of η_2-H_2 bound at the distal iron of the $Fe^{II}Fe^{II}$ redox level to the central nitrogen of the DTMA linker to be +5.6, −2.6, and −7.7 kcal/mol, respectively, when dielectric constant values (ϵ) of 1 (gas-phase), 4, and 40 are used for the solvation calculations. For the transfer of H^+ from the $H-Fe^{II}Fe^{II}$ to yield the $Fe^{I}Fe^{I}$ form, they compute values of +15.6, +9.5, and +4.7 kcal/mol, respectively, for $\epsilon = 1$, 4, and 40.

The work of De Gioia and co-workers initially suggested a catalytic cycle for H_2 oxidation such as the one given in Figure 24.[143−145] This cycle begins with the inactive, over-oxidized form of [FeFe]H_2ase derived from DdH that corresponds to an $Fe^{II}Fe^{II}$ redox level with OH^- bound at the distal iron center. Protonation of the OH^- ligand and one-electron reduction leads to loss of the bound H_2O yielding a

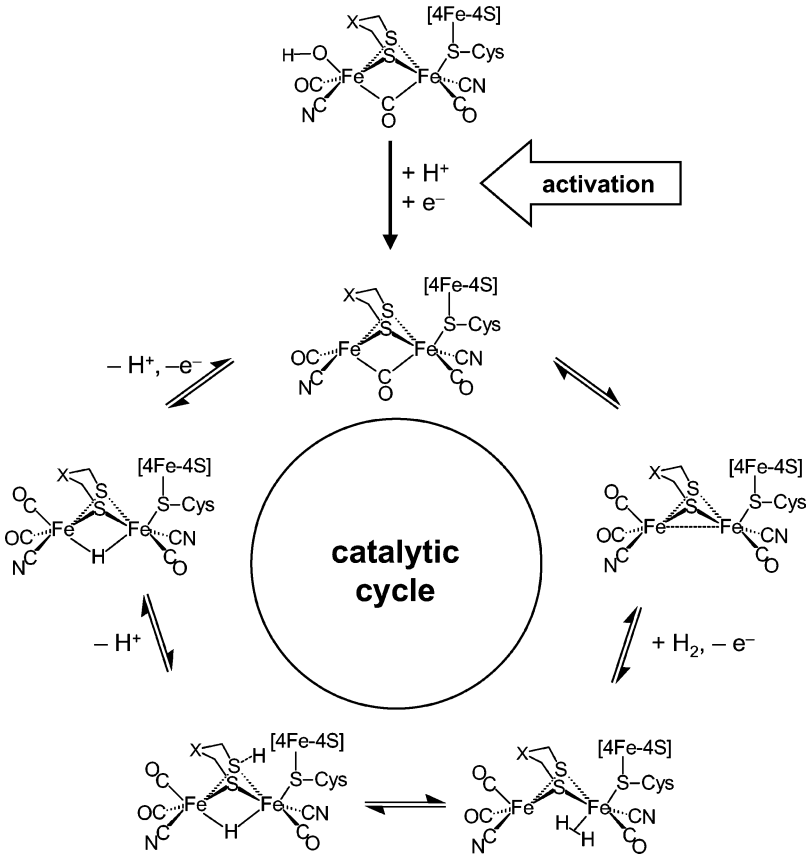

Figure 24. Proposed catalytic cycle for [FeFe]H_2ase featuring rearrangement of the enzyme active site. The oxidation states have been left purposely ambiguous.

catalytically active $Fe^{I}Fe^{II}$ form. The μ-CO $Fe^{I}Fe^{II}$ form rearranges to a form with all-terminal CO ligands. Dihydrogen binds to the proximal iron center, and the complex undergoes a one-electron oxidation to yield an Fe^{II} (η_2-H_2)-Fe^{II} form. A proton is transferred from the bound η_2-H_2 to a sulfur atom of the bridging dithiolate. The sulfur- and iron-bound protons are moved away from the di-iron active site by the protein. The di-iron active site undergoes one-electron oxidation to $Fe^{I}Fe^{II}$ to close the catalytic cycle.

The work of Hall, Hu, and their respective co-workers suggests a catalytic cycle for H_2 oxidation such as the one given in Figure 25. This cycle begins with the inactive, overoxidized form of [FeFe]H_2ase derived from DdH that corresponds to an $Fe^{II}Fe^{II}$ redox level with OH^- bound at the distal iron center. Protonation of the OH^- ligand and one-electron reduction leads to loss of the bound H_2O yielding a catalytically active $Fe^{I}Fe^{II}$ form. Dihydrogen binds to the distal iron center, and the complex undergoes a one-electron oxidation to yield an (η_2-H_2)$Fe^{II}Fe^{II}$ form. A proton is transferred from the bound η_2-H_2 to a nitrogen of the μ-SCH_2NHCH_2S and then moved away from the di-iron active site by the protein. The second proton is transferred from the hydride ligand to the nitrogen of the μ-SCH_2-$NHCH_2S$ and then moved away from the di-iron active site by the protein. The di-iron active site undergoes one-electron oxidation to $Fe^{I}Fe^{II}$ to close the catalytic cycle.

The mechanisms presented in Figures 24 and 25 should not be taken to imply that the order of proton- and electron-transfer events is known or that discrete proton- and electron-transfer events are known to occur. In fact, the [FeFe]H_2ase mechanism may involve simultaneous proton−electron transfers rather than discrete proton-transfer and electron-transfer steps. Figure 26 shows the H_{ox} and H_{red} active forms of [FeFe]H_2ase interconverting directly by proton-coupled electron transfer without other intermediates being formed. As shown in Figure 26, the binding of H_2 to the $Fe^{I}Fe^{II}$ H_{ox} form may trigger simultaneous proton−electron transfer to yield an H−$Fe^{II}Fe^{II}$ H_{red} form. The H−$Fe^{II}Fe^{II}$ form H_{red} may then undergo a simultaneous proton−electron transfer to regenerate the $Fe^{I}Fe^{II}$ H_{ox} form. This type of interconversion is in agreement with the experimental results of Albracht et al. that show that the H_{red} form is in equilibrium with H_{ox} + H_2 (i.e., $H_{red} \leftrightarrow H_{ox} + H_2$).[128]

4. Conclusions

The present status of computational modeling of [NiFe] and [FeFe] hydrogenases has been reviewed. For the mechanism of the heterolytic cleavage of the H−H bond in dihydrogen, a high degree of consensus has been reached during the past years. Still, some issues remain controversial, and in some cases severe and, so far, unresolved problems remain in the modeling.

For [NiFe] hydrogenases, most studies agree that the heterolytic cleavage of the H−H bond leads to a bridging hydride and a protonated terminal Cys492, following a transition state as shown in Figure 4. Protonation of another cysteine is possible but appears less likely at this stage. Different opinions still exist about whether it is the $Ni^{II}Fe^{II}$ or the $Ni^{III}Fe^{II}$ state that is active in cleaving the bond. If the $Ni^{II}Fe^{II}$ state is active, the dihydrogen cleavage is suggested to connect the two EPR-silent states Ni_a-S and Ni_a-SR, which have been observed. Electron and proton release from the complex leads to the suggested structure for the EPR-active state Ni_a-C*, which is the resting state

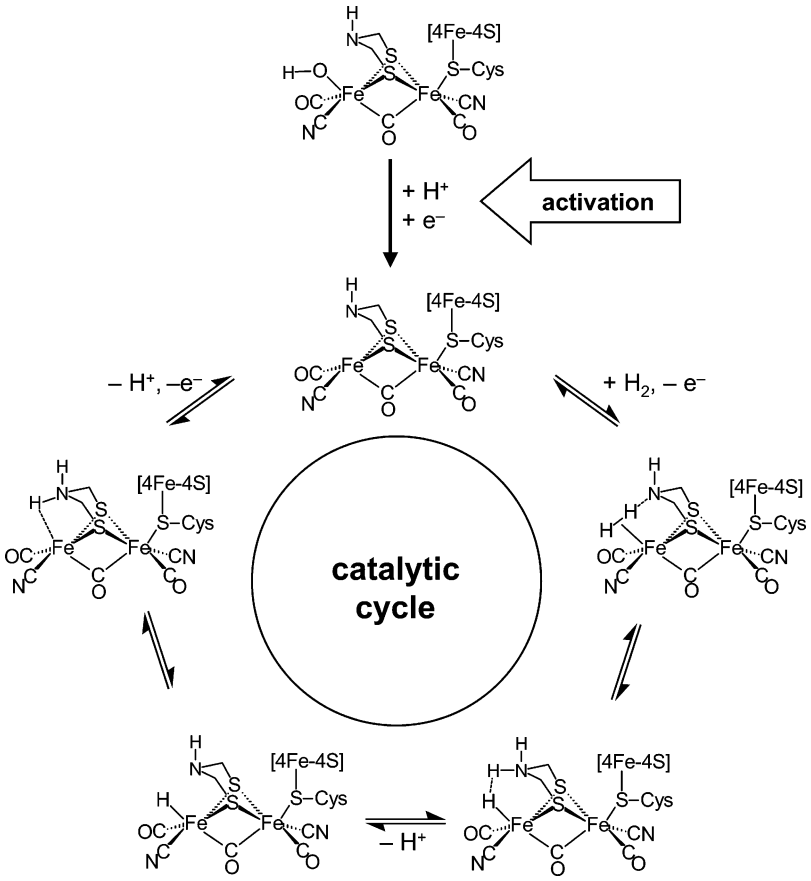

Figure 25. Proposed catalytic cycle for [FeFe]H_2ase using the central nitrogen of the μ-SCH_2NHCH_2S linker for H^+ transfer. The oxidation states have been left purposely ambiguous.

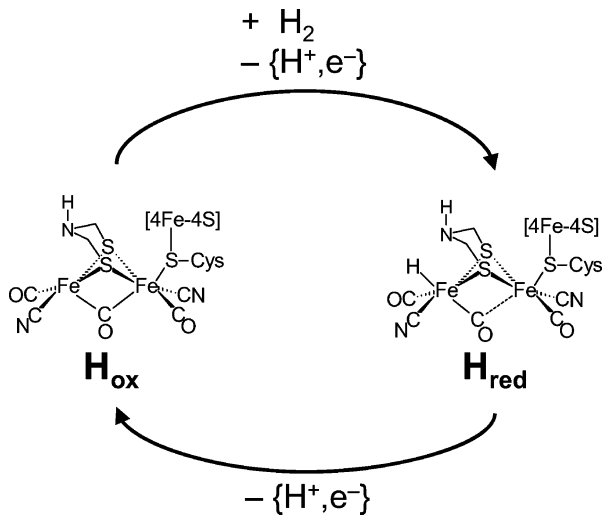

Figure 26. Direct conversion between the H_{ox} and H_{red} forms. In the mechanism, the H_{ox} and H_{red} forms interconvert via simultaneous proton−electron transfers.

of the catalytic cycle (see Figures 7 and 8). The catalytic cycle then continues by a hydride transfer from the bridging position to Cys492, where nickel is reduced from Ni^{III} to Ni^{I}, a key step in the cycle which is at least as critical as the dihydrogen cleavage. A proton and an electron release completes the cycle.

For the [NiFe] hydrogenase, the most difficult system to model has been the oxidized Ni-A state. It has only quite recently been demonstrated experimentally that this state has a protonated peroxide in between nickel and iron in an unusual side-on binding mode to nickel. The computational studies where this state is compared to a bridging but end-on bonded protonated peroxide have so far favored the latter structure in conflict with experimental data. The failure of the modeling in this case is very unusual and is probably not connected with the use of DFT but with the chemical model used. Large models of QM/MM type may be required to adequatly describe these states.

Calculations on [FeFe] hydrogenase models strongly support a cycle which involves reduction of the $Fe^{I}Fe^{II}$ resting form to the $Fe^{I}Fe^{I}$ form then capture of a proton by the metal(s), an event that oxidizes the metals to an $Fe^{II}Fe^{II}$ form. A second proton and electron transfer produces dihydrogen and regenerates the $Fe^{I}Fe^{II}$ form. One major controversy revolves around the structural integrity of the active site, i.e., whether the bridging CO ligand observed in both enzyme structures can move to the axial site. Calculations favor this geometry for the reduced state, and it is the geometry observed in synthetic model complexes. If this structure is accessible in the enzyme, dihydrogen formation would most likely occur between the two metals. However, if the enzyme structure is more rigid, then the CO would remain in the bridging site and dihydrogen production would take place at the distal Fe. Although the exact nature of the five-atom dithiolate linker is not known, the transition state calculations show that the proposed amine linker would provide a very suitable base for proton transfer to the distal Fe.

5. References

(1) Penner, S. S. *Energy* **2006**, *31*, 33.
(2) Artero, V.; Fontecave, M. *Coord. Chem. Rev.* **2005**, *249*, 1518.
(3) Best, S. P. *Coord. Chem. Rev.* **2005**, 249, 1536.
(4) Bouwman, E.; Reedijk, J. *Coord. Chem. Rev.* **2005**, *249*, 1555.

(5) Evans, D. J. *Coord. Chem. Rev.* **2005**, *249*, 1582.
(6) de Lacey, A. L.; Fernandez, V. M.; Rousset, M. *Coord. Chem. Rev.* **2005**, *249*, 1596.
(7) Volbeda, A.; Fontecilla-Camps, J. C. *Coord. Chem. Rev.* **2005**, *249*, 1609.
(8) Bruschi, M.; Zampella, G.; Fantucci, P.; De Gioia, L. *Coord. Chem. Rev.* **2005**, *249*, 1620.
(9) Liu, X.; Ibrahim, S. K.; Tard, C.; Pickett, C. J. *Coord. Chem. Rev.* **2005**, *249*, 1641.
(10) Sun, L.; Åkermark, B.; Ott, S. *Coord. Chem. Rev.* **2005**, *249*, 1653.
(11) Capon, J.-F.; Gloaguen, F.; Schollhammer, P.; Talarmin, J. *Coord. Chem. Rev.* **2005**, *249*, 1664.
(12) Vignais, P. M. *Coord. Chem. Rev.* **2005**, *249*, 1677.
(13) Henderson, R. A. *Coord. Chem. Rev.* **2005**, *249*, 1841.
(14) Tye, J. W.; Hall, M. B.; Darensbourg, Marcetta, Y. *Proc. Natl. Acad. Sci. U.S.A.* **2005**, *102*, 16911.
(15) Vincent, K. A.; Cracknell, J. A.; Parkin, A.; Armstrong, F. A. *Dalton Trans.* **2005**, 3397.
(16) Pickett, C. J. *Trends Mol. Electrochem.* **2004**, 209.
(17) Georgakaki, I. P.; Darensbourg, M. Y. In *Comprehensive Coordination Chemistry 2*; McCleverty, J. A., Meyer, T. J., Eds.; Elsevier: Oxford, 2003; Vol. 8, pp 569.
(18) Evans, D. J.; Pickett, C. J. *Chem. Soc. Rev.* **2003**, *32*, 268.
(19) Frey, M.; Fontecilla-Camps, J. C. In *Handbook of Metalloproteins*; Messerschmidt, A., Huber, R., Poulos, T., Wieghardt, K., Eds.; John Wiley & Sons: Chichester, U.K., 2001; Vol. 2, pp 880.
(20) Lemon, B. J.; Peters, J. W. In *Handbook of Metalloproteins*; Messerschmidt, A., Huber, R., Poulos, T., Wieghardt, K., Eds.; John Wiley & Sons: Chichester, U.K., 2001; Vol. 2, pp 738.
(21) Marr, A. C.; Spencer, D. J. E.; Schroder, M. *Coord. Chem. Rev.* **2001**, *219*−*221*, 1055.
(22) Darensbourg, M. Y.; Lyon, E. J.; Smee, J. J. *Coord. Chem. Rev.* **2000**, *206*−*207*, 533.
(23) *Transition Metal Hydrides*; Dedieu, A., Ed.; VCH: New York, 1992.
(24) *Metal Dihydrogen and σ-Bond Complexes: Structure, Theory and Reactivity*; Kubas, G. J., Ed.; Kluwer Academic/Plenum Publishers: Dordrecht, Netherlands, 2001.
(25) *Recent Advances in Hydride Chemistry*; Peruzzini, M., Poli, R., Eds.; Elsevier: Amsterdam, 2001.
(26) Kubas, G. J. J. *Less-Common Metals* **1991**, *173*, 475.
(27) Espinet, P.; Esteruelas, M. A.; Oro, L. A.; Serrano, J. L.; Sola, E. *Coord. Chem. Rev.* **1992**, *117*, 215.
(28) Jessop, P. G.; Morris, R. H. *Coord. Chem. Rev.* **1992**, *121*, 155.
(29) Heinekey, D. M.; Oldham, W. J., Jr. *Chem. Rev.* **1993**, *93*, 913.
(30) Kuhlman, R. *Coord. Chem. Rev.* **1997**, 167, 205.
(31) Crabtree, R. H. *J. Organomet. Chem.* **1998**, *557*, 111.
(32) Crabtree, R. H.; Eisenstein, O.; Sini, G.; Peris, E. *J. Organomet. Chem.* **1998**, *567*, 7.
(33) Esteruelas, M. A.; Oro, L. A. *Chem. Rev.* **1998**, *98*, 577.
(34) Sabo-Etienne, S.; Chaudret, B. *Coord. Chem. Rev.* **1998**, *178*−*180*, 381.
(35) Sabo-Etienne, S.; Chaudret, B. *Chem. Rev.* **1998**, *98*, 2077.
(36) Jia, G.; Lau, C.-P. *Coord. Chem. Rev.* **1999**, *190*−*192*, 83.
(37) Maseras, F.; Lledos, A.; Clot, E.; Eisenstein, O. *Chem. Rev.* **2000**, *100*, 601.
(38) McGrady, G. S.; Guilera, G. *Chem. Soc. Rev.* **2003**, *32*, 383.
(39) Heinekey, D. M.; Lledos, A.; Lluch, J. M. *Chem. Soc. Rev.* **2004**, *33*, 175.
(40) Bakhmutov, V. I. *Eur. J. Inorg. Chem.* **2005**, 245.
(41) Zhang, X.-M.; Bruno, J. W.; Enyinnaya, E. *J. Org. Chem.* **1998**, *63*, 4671.
(42) Darwent, B. *Natl. Stand. Ref. Data Ser. Natl. Bur. Stand.* **1970**, (NSRDS-NBS 31).
(43) Abdur-Rashid, K.; Fong, T. P.; Greaves, B.; Gusev, D. G.; Hinman, J. G.; Landau, S. E.; Lough, A. J.; Morris, R. H. *J. Am. Chem. Soc.* **2000**, *122*, 9155.
(44) Izutsu, K. *Acid-Base Dissociation Constants in Dipolar Aprotic Solvents*; Blackwell Scientific Publications: Oxford, 1990; Vol. 35.
(45) Kolthoff, I. M.; Chantooni, M. K., Jr. *J. Chem. Eng. Data* **1999**, *44*, 124.
(46) Przbyla, A. E.; Robbins, J.; Menon, N.; Peck, H. D., Jr. *FEMS Microbiol. Rev.* **1992**, *8*, 109-13.
(47) Garcin, E.; Vernede, X.; Hatchikian, E. C.; Volbeda, A.; Frey M.; Fontecilla-Camps, J. C. *Structure* **1999**, *7*, 557.
(48) Teixeira, M.; Moura, I.; Xavier, A. V.; Huynh, B. H.; DerVartanian, D. V.; Peck, H. D., Jr.; LeGall, J.; Moura, J. J. G. *J. Biol. Chem.* **1985**, *260*, 8942.
(49) Nicolet, Y.; Lemon, B. J.; Fontecilla-Camps, J. C.; Peters, J. W. *Trends Biochem. Sci.* **2000**, *25*, 138.
(50) Peters, J. W. *Curr. Opin. Struct. Biol.* **1999**, *9*, 670.
(51) Lyon, E. J.; Shima, S.; Buurman, G.; Chowdhuri, S.; Batschauer, A.; Steinbach, K.; Thauer, R. K. *Eur. J. Biochem.* **2004**, *271*, 195.
(52) Berkessel, A.; Thauer, R. K. *Angew. Chem., Int. Ed. Engl.* **1995**, *34*, 2247.
(53) Thauer, R. K.; Klein, A. R.; Hartmann, G. C. *Chem. Rev.* **1996**, *96*, 3031.
(54) Lyon, E. J.; Shima, S.; Boecher, R.; Thauer, R. K.; Grevels, F.-W.; Bill, E.; Roseboom, W.; Albracht, S. P. J. *J. Am. Chem. Soc.* **2004**, *126*, 14239.
(55) Vignais, P. M.; Dimon, B.; Zorin, N. A.; Tomiyama, M.; Colbeau, A. *J. Bacteriol.* **2000**, *182*, 5997.
(56) Bernhard, M.; Buhrke, T.; Bleijlevens, B.; De Lacey, A. L.; Fernandez, V. M.; Albracht, S. P. J.; Friedrich, B. *J. Biol. Chem.* **2001**, *276*, 15592.
(57) Volbeda, A.; Charon, M. H.; Piras, C.; Hatchikian, E. C.; Frey, M.; Fontecilla-Camps, J. C. *Nature* **1995**, *373*, 580.
(58) Volbeda, A.; Garcin, E.; Piras, C.; de Lacey, A. L.; Fernandez, V. M.; Hatchikian, E. C.; Frey, M.; Fontecilla-Camps, J. C. *J. Am. Chem. Soc.* **1996**, *118*, 12989.
(59) Rousset, M.; Montet, Y.; Guigliarelli, B.; Forget, N.; Asso, M.; Bertrand, P.; Fontecilla-Camps, J. C.; Hatchikian, E. C. *Proc. Natl. Acad. Sci. U.S.A.* **1998**, *95*, 11625.
(60) Higuchi, Y.; Yagi, T.; Yasuoka, N. *Structure* **1997**, *5*, 1671.
(61) Higuchi, Y.; Ogata, H.; Miki, K.; Yasuoka, N.; Yagi, T. *Structure* **1999**, *7*, 549.
(62) Ogata, H.; Mizoguchi, Y.; Mizuno, N.; Miki, K.; Adachi, S.-I.; Yasuoka, N.; Yagi, T.; Yamauchi, O.; Hirota, S.; Higuchi, Y. *J. Am. Chem. Soc.* **2002**, *124*, 11628.
(63) Volbeda, A.; Martin, L.; Cavazza, C.; Matho, M.; Faber, B. W.; Roseboom, W.; Albracht, S. P. J.; Garcin, E.; Rousset, M.; Fontecilla-Camps, J. C. *J. Biol. Inorg. Chem.* **2005**, *10*, 239.
(64) Ogata, H.; Hirota, S.; Nakahara, A.; Komori, H.; Shibata, N.; Kato, T.; Kano, K.; Higuchi, Y. *Structure* **2005**, *13*, 1635.
(65) Happe, R. P.; Roseboom, W.; Pierik, A. J.; Albracht, S. P. J.; Bagley, K. A. *Nature* **1997**, *385*, 126.
(66) Dobbek, H.; Svetlitchnyi, V.; Gremer, L.; Huber, R.; Meyer, O. *Science* **2001**, *293*, 1281.
(67) Drennan, C. L.; Heo, J.; Sintchak, M. D.; Schreiter, E.; Ludden, P. W. *Proc. Natl. Acad. Sci. U.S.A.* **2001**, *98*, 11973.
(68) Pelmenschikov, V.; Blomberg, M. R. A.; Siegbahn, P. E. M. *J. Biol. Inorg. Chem.* **2002**, *7*, 284.
(69) Siegbahn, P. E. M. *Adv. Inorg. Chem.* **2004**, *56*, 101.
(70) Siegbahn, P. E. M.; Borowski, T. *Acc. Chem. Res.* **2006**, *39*, 729.
(71) Amara, P.; Volbeda, A.; Fontecilla-Camps, J. C.; Field, M. J. *J. Am. Chem. Soc.* **1999**, *121*, 4468.
(72) Söderhjelm, P.; Ryde, U. *THEOCHEM* **2006**, *770*, 199.
(73) Dole, F.; Fournel, A.; Magro, V.; Hatchikian, E. C.; Bertrand, P.; Guigliarelli, B. *Biochemistry* **1997**, *36*, 7847.
(74) Wang, C. P.; Franco, R.; Moura, J. J. G.; Moura, I.; Day, E. P. *J. Biol. Chem.* **1992**, *267*, 7378.
(75) Kowal, A. T.; Zambrano, I. C.; Moura, I.; Moura, J. J. G.; LeGall, J.; Johnsson, M. K. *Inorg. Chem.* **1988**, *27*, 1162.
(76) Wang, H.; Ralston, C. Y.; Patil, D. S.; Jones, R. M.; Gu, W.; Verhagen, M.; Adams, M.; Ge, P.; Riordan, C.; Marganian, C. A.; Mascharak, P.; Kovacs, J.; Miller, C. G.; Collins, T. J.; Brooker, S.; Croucher, P. D.; Wang, K.; Stiefel, E. I.; Cramer, S. P. *J. Am. Chem. Soc.* **2000**, *122*, 10544.
(77) Fan, H.-J.; Hall, M. B. *J. Am. Chem. Soc.* **2002**, *124*, 394.
(78) Bruschi, M.; De Gioia, L.; Zampella, G.; Reiher, M.; Fantucci, P.; Stein, M. *J. Biol. Inorg. Chem.* **2004**, *9*, 873.
(79) Reiher, M.; Salomon, O.; Hess, B. A. *Theor. Chem. Acc.* **2001**, *107*, 48.
(80) Albracht, S. P. J. *Biochim. Biophys. Acta* **1994**, *1188*, 167.
(81) DeGioia, L.; Fantucci, P.; Guigliarelli, B.; Bertrand, P. *Int. J. Quantum Chem.* **1999**, *73*, 187.
(82) De Gioia, L.; Fantucci, P.; Guigliarelli, B.; Bertrand, P. *Inorg. Chem.* **1999**, *38*, 2658.
(83) Pavlov, M.; Siegbahn, P. E. M.; Blomberg, M. R. A.; Crabtree, R. H. *J. Am. Chem. Soc.* **1998**, *120*, 548.
(84) Pavlov, M.; Blomberg, M. R. A.; Siegbahn, P. E. M. *Int. J. Quantum Chem.* **1999**, *73*, 197.
(85) Siegbahn, P. E. M.; Blomberg, M. R. A.; Wirstam, M.; Crabtree, R. H. *J. Biol. Inorg. Chem.* **2001**, *6*, 460.
(86) Niu, S. Q.; Thomson L. M.; Hall, M. B. *J. Am. Chem. Soc.* **1999**, *121*, 4000.
(87) Fan, H.-J.; Hall, M. B. *J. Biol. Inorg. Chem.* **2001**, *6*, 467.
(88) Li, S.; Hall, M. B. *Inorg. Chem.* **2001**, *40*, 18.
(89) Niu, S.; Hall, M. B. *Inorg. Chem.* **2001**, *40*, 6201.
(90) Wirstam, M.; Lippard, S. J.; Friesner, R. A. *J. Am. Chem. Soc.* **2003**, *125*, 3980.
(91) Montet, Y.; Amara, P.; Volbeda, A.; Vernede, X.; Hatchikian, E. C.; Field, M. J.; Frey, M.; Fontecilla-Camps, J. C. *Nat. Struct. Biol.* **1997**, *4*, 523.
(92) Volbeda, A.; Fontecilla-Camps *Dalton Trans.* **2003**, 4030.

(93) Siegbahn, P. E. M.; Blomberg, M. R. A. In *Theoretical Aspects of Homogeneous Catalysis, Applications of Ab Initio Molecular Orbital Theory*; van Leeuwen, P. W. N. M., van Lenthe, J. H., Morokuma, K., Ed.; Kluwer Academic/Plenum Publishers: Dordrecht, Netherlands, 1993.
(94) Pardo, A.; de Lacey, A.; Fernandez, V. M.; Fan, Y.; Hall, M. B. *J. Biol. Inorg. Chem.* **2006**, *11*, 286.
(95) Stein, M.; Lubitz, W. *J. Inorg. Biochem.* **2004**, *98*, 862.
(96) Stein, M.; Lubitz, W. *Curr. Opin. Chem. Biol.* **2002**, *6*, 243.
(97) Maroney, M. J.; Bryngelson, P. A. *J. Biol. Inorg. Chem.* **2001**, *6*, 453.
(98) Siegbahn, P. E. M. *J. Biol. Inorg. Chem.* **2006**, *11*, 695.
(99) Stein, M.; van Lenthe, E.; Baerends, E. J.; Lubitz, W. *J. Am. Chem. Soc.* **2001**, *123*, 5839.
(100) Foerster, S.; Stein, M.; Brecht, M.; Ogata, H.; Higuchi, Y.; Lubitz, W. *J. Am. Chem. Soc.* **2003**, *125*, 83.
(101) Blomberg, M. R. A.; Siegbahn, P. E. M. *J. Comp. Chem.* **2006**, *27*, 1373.
(102) Siegbahn, P. E. M.; Lundberg, M. *J. Inorg. Biochem.* **2006**, *100*, 1035.
(103) Jayapal, P.; Sundararajan, M.; Hillier, I. H.; Burton, N. A. *Phys. Chem. Chem. Phys.* **2006**, *8*, 4086.
(104) Pardo, A.; de Lacey, A.; Fernandez, V. M.; Fan, Y.; Hall, M. B. *J. Biol. Inorg. Chem.* **2007**, in press.
(105) Siegbahn, P. E. M. *C. R. Chimie* **2007**, http://dx.doi.org/10.1016/j.crci.2007.03.011.
(106) Stein, M.; Lubitz, W. *Phys. Chem. Chem. Phys.* **2001**, *3*, 2668.
(107) Stadler, C.; de Lacey, A. L.; Montet, Y.; Volbeda, A.; Fontecilla-Camps, J. C.; Conesa, J. C.; Fernandez, V. M. *Inorg. Chem.* **2002**, *41*, 4424.
(108) Siegbahn, P. E. M. *Q. Rev. Biophys.* **2003**, *36*, 91.
(109) Siegbahn, P. E. M. *J. Comp. Chem.* **2001**, *22*, 1634.
(110) Kurkin, S.; George, S. J.; Thorneley, R. N. F.; Albracht, S. P. J. *Biochemistry* **2004**, *43*, 6820.
(111) Lamle, S. E.; Albracht, S. P. J.; Armstrong, F. A. *J. Am. Chem. Soc.* **2004**, *126*, 14899.
(112) Lamle, S. E.; Albracht, S. P. J.; Armstrong, F. A. *J. Am. Chem. Soc.* **2005**, *127*, 6595.
(113) van Gastel, M.; Stein, M.; Brecht, M.; Schröder, O.; Lendzian, F.; Bittl, R.; Ogata, H.; Higuchi, Y.; Lubitz, W. J. *Biol. Inorg. Chem.* **2006**, *11*, 41.
(114) Adams, M. W. W. *Biochim. Biophys. Acta* **1990**, *115*, 1020.
(115) Frey, M. *Structure and Bonding*; Springer-Verlag: Berlin, Heidelberg, 1998; Vol. 97, p 90.
(116) Peters, J. W.; Lanzilotta, W. N.; Lemon, B. J.; Seefedt, L. C. *Science* **1998**, *282*, 1853. (Errata: Science *283*, 35; *283*, 2102.) (Protein Data Bank code 1FEH.)
(117) Lemon, B. J.; Peters, J. W. *Biochemistry* **1999**, *38*, 12969. (Protein Data Bank codes 1C4A and 1C4C.)
(118) Nicolet, Y.; Piras, C.; Legrand, P.; Hatchikian, C. E.; Fontecilla-Camps, J. C. *Structure* **1999**, *7*, 13. (Protein Data Bank code 1HFE.)
(119) Nicolet, Y.; De Lacey, A. L.; Vernede, X.; Fernandez, V. M.; Hatchikian, E. C.; Fontecilla-Camps, J. C. *J. Am. Chem. Soc.* **2001**, *123*, 1596.
(120) Nicolet, Y.; Cavazza, C.; Fontecilla-Camps, J. C. *J. Inorg. Biochem.* **2002**, *91*, 1.
(121) Adams, M. W. W.; Mortenson, L. E. *J. Biol. Chem.* **1984**, *259*, 7045.
(122) Adams, M. W. W. *J. Biol. Chem.* **1987**, *262*, 15054.
(123) Zambrano, I. C.; Kowal, A. T.; Mortenson, L. E.; Adams, M. W. W.; Johnson, M. K. *J. Biol. Chem.* **1989**, *264*, 20974.
(124) Bennett, B.; Lemon, B. J.; Peters, J. W. *Biochemistry* **2000**, *39*, 7455.
(125) Pierik, A. T.; Hulstein, M.; Hagen, W. R.; Albracht, S. P. J. *Eur. J Biochem.* **1998**, *258*, 572.
(126) De Lacey, A. L.; Stadler, C.; Cavazza, C.; Hatchikian, E. C.; Fernandez, V. M. *J. Am. Chem. Soc.* **2000**, *122*, 11232.
(127) Chen, Z.; Lemon, B. J.; Huang, S.; Swartz, D. J.; Peters, J. W.; Bagley, K. A. *Biochemistry* **2002**, *41*, 2036.
(128) (a) Roseboom, W.; De Lacey, A. L.; Fernandez, V. M.; Hatchikian, E. C.; Albracht, S. P. J. *J. Biol. Inorg. Chem.* **2006**, *11*, 102. (b) Albracht, S. P. J.; Roseboom, W.; Hatchikian, E. C. *J. Biol. Inorg. Chem.* **2006**, *11*, 88.
(129) (a) Reihlen, H.; Gruhl, A.; v. Hessling, G. *Ann.* **1929**, it *472*, 268. (b) Hieber, W.; Spacu, P. Z. *Anorg. Allg. Chem.* **1937**, *233*, 353. (c) Fauvel, K.; Mathieu, R.; Poilblanc, R. *Inorg. Chem.* **1976**, *15*, 976. (d) Seyferth, D.; Henderson, R. S.; Song, L. C. *Organometallics* **1982**, *1*, 125. (e) Winter, A.; Zsolnai, L.; Huttner, G. *Z. Naturforsch., B: Chem. Sci.* **1982**, *37B*, 1430. (f) Treichel, P. M.; Rublein, E. K. *J. Organomet. Chem.* **1989**, *359*, 195. (g) Seyferth, D.; Womack, G. B.; Gallagher, M. K.; Cowie, M.; Hames, B. W.; Fackler, J. P., Jr.; Mazany, A. M. *Organometallics* **1987**, *6*, 283.
(130) (a) Lyon, E. J.; Georgakaki, I. P.; Reibenspies, J. H.; Darensbourg, M. Y. *Angew. Chem., Int. Ed. Engl.* **1999**, *38*, 3178. (b) Schmidt, M.; Contakes, S. M.; Rauchfuss, T. B. *J. Am. Chem. Soc.* **1999**, *121*, 9736. (c) Cloirec, A. L.; Davies, S. C.; Evans, D. J.; Hughes, D. L.; Pickett, C. J.; Best, S. P.; Borg, S. *Chem. Commun.* **1999**, 2285.
(131) Rusnak, F. M.; Adams, M. W. W.; Mortenson, L. E.; Münck, E. *J. Biol. Chem.* **1987**, *262*, 38.
(132) Popescu, C. V.; Münck, E. *J. Am. Chem. Soc.* **1999**, *121*, 7877.
(133) Pereira, A. S.; Tavares, P.; Moura, I.; Moura, J. J. G.; Huynh, B. H. *J. Am. Chem. Soc.* **2001**, *123*, 2771.
(134) Cao, Z.; Hall, M. B. *J. Am. Chem. Soc.* **2001**, *123*, 3734.
(135) Nakamoto, K. *IR and Raman Spectra of Inorganic and Coordination Compounds*, 5th ed.; Wiley-Interscience: New York, 1997; Parts A and B.
(136) Fiedler, A. T.; Brunold, T. C. *Inorg. Chem.* **2005**, *44*, 9322.
(137) Zilberman, S.; Stiefel, E. I.; Cohen, M. H.; Car, R. *Inorg. Chem.* **2006**, *45*, 5715.
(138) Dance, I. *Chem. Commun.* **1999**, 1655.
(139) Fan, H.-J.; Hall, M. B. *J. Am. Chem. Soc.* **2001**, *123*, 3828.
(140) Liu, Z.-P.; Hu, P *J. Am. Chem. Soc.* **2002**, *124*, 5175.
(141) Liu, Z.-P.; Hu, P. *J. Chem. Phys.* **2002**, *117*, 8177.
(142) Zhou, T.; Mo, Y.; Zhou, Z.; Tsai, K. *Inorg. Chem.* **2005**, *44*, 4941.
(143) Bruschi, M.; Fantucci, P.; De Gioia, L. *Inorg. Chem.* **2002**, *41*, 1421.
(144) Bruschi, M.; Fantucci, P.; De Gioia, L. *Inorg. Chem.* **2003**, *42*, 4773.
(145) Zampella, G.; Greco, C.; Fantucci, P.; De Gioia, L. *Inorg. Chem* **2006**, *45*, 4109.

CR050185Y